



**NANYANG
TECHNOLOGICAL
UNIVERSITY**
SINGAPORE

Low Temperature Carbon/Nitrogen Plasma Engineered High-performance Electrocatalyst for Energy Storage and Conversion

Rajdeep S Rawat

**Plasma Engineering and Applied Research Lab (PEARL) &
Plasma Radiation Sources Lab (PRSL)**

National Institute of Education, NTU, Singapore

19-22 Sep 2023

IAEA Technical Meeting on Emerging Applications
of Plasma Science and Technology



Outline of Presentation

Introduction – Energy Conversion and Plasmas,

- Hydrogen Economy (Energy Conversion)
- Electrocatalysis
- Plasma processing for EC-Energy conversion/~~storage~~ Materials

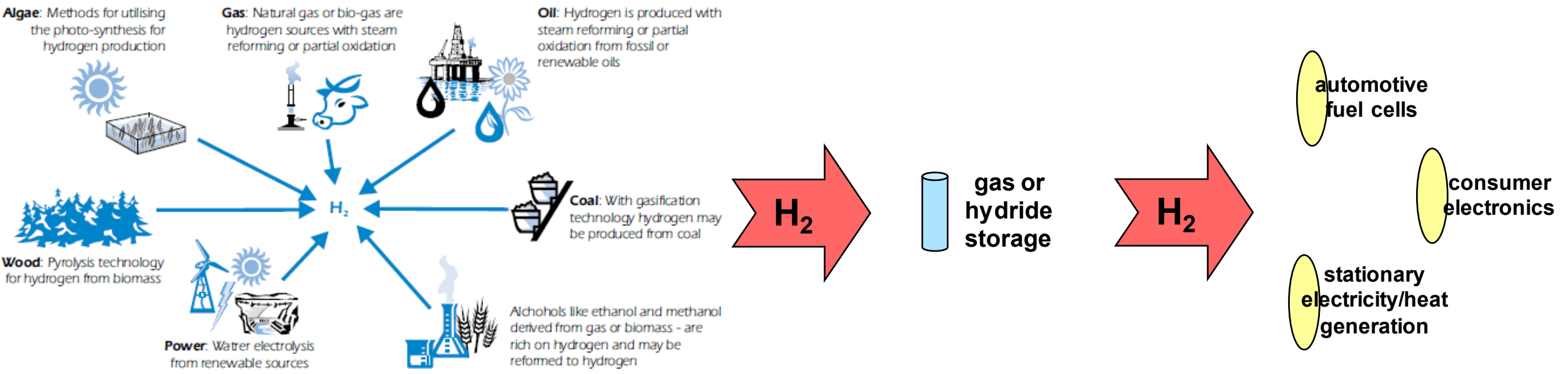
Some examples of application of low temperature nitrogen/carbon plasmas for energy conversion applications

Recent Work - Facet Control of Ni₃N Nano-Framework for Efficient HER via Auxiliary Cooling Assisted Plasma Engineering

Conclusions

Acknowledgement: Bo Ouyang, Yongqi Zhong, Chao Dongliang, Fan Hongjin (all NTU Singapore), Zhang Zheng (A*Star, Singapore) & Erjan Kan (NJUST, China)

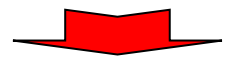
Energy Conversion - Hydrogen Economy



Source: Hydro.

production

9 M tons/yr



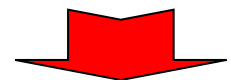
150 M tons/yr

(light trucks and cars in 2040)

storage

4.4 MJ/L (Gas, 10,000 psi)

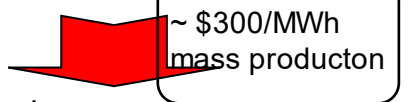
8.4 MJ/L (LH2)



9.72 MJ/L

use in fuel cells





\$3000/MWh



\$30/MWh

(Internal Combustion Engine)

Type of Hydrogen

Color	GREY HYDROGEN	BLUE HYDROGEN	TURQUOISE HYDROGEN*	GREEN HYDROGEN
Process	SMR or gasification	SMR or gasification with carbon capture (85-95%)	Pyrolysis	Electrolysis
Source	Methane or coal 	Methane or coal 	Methane 	Renewable electricity 

Green hydrogen – also referred to as “clean hydrogen” – is produced by using clean energy from surplus renewable energy sources, such as solar or wind power, to split water into two hydrogen atoms and one oxygen atom through a process called electrolysis.

It currently makes up about <1% of overall hydrogen production, but this is expected to rise as the cost of renewable energy continues to fall.

Note: SMR = steam methane reforming.

* Turquoise hydrogen is an emerging decarbonisation option.

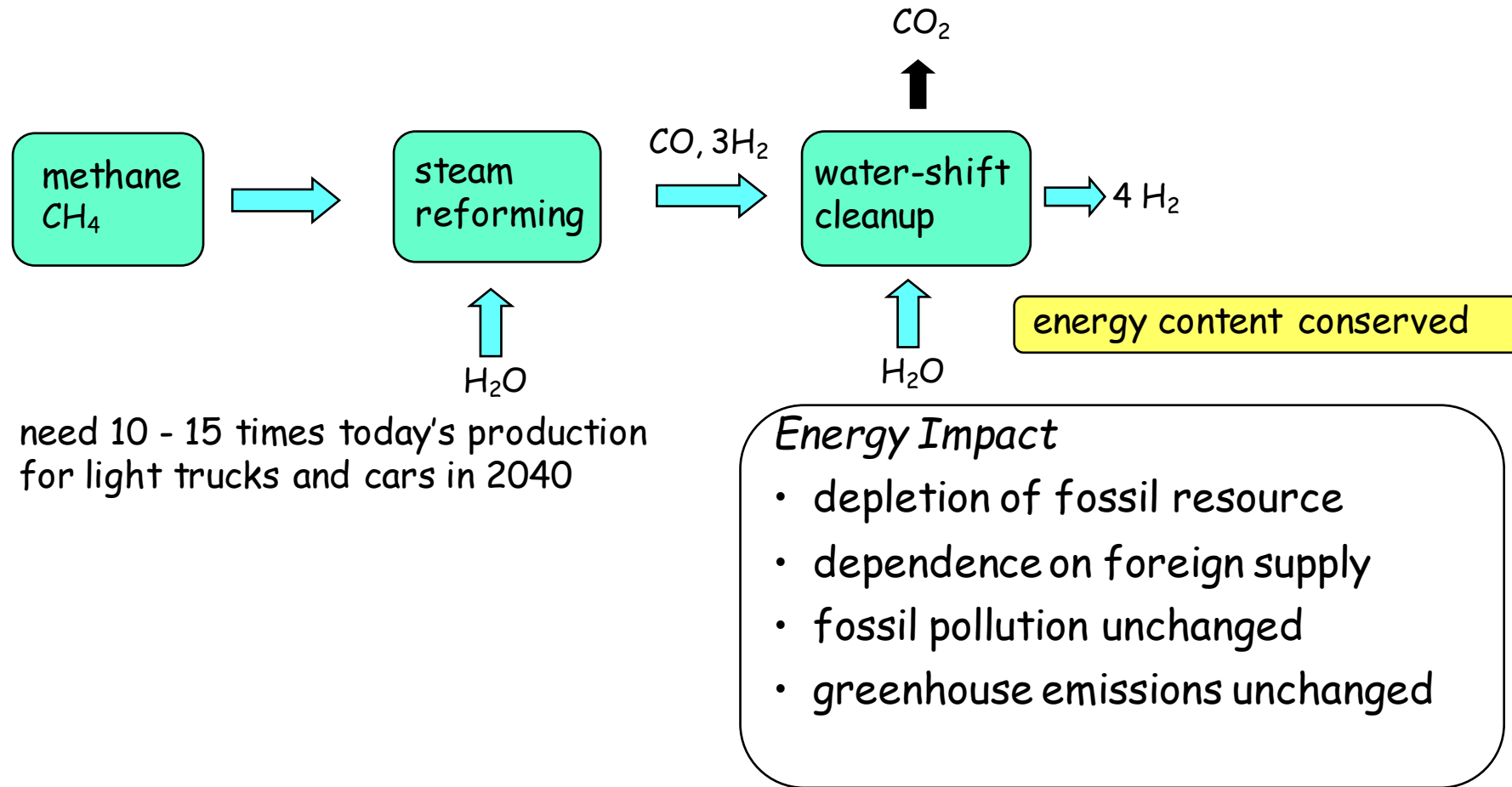
Grey hydrogen: most common form; generated from natural gas, or methane, through a process called “steam reforming”; generates smaller amount of emissions than black (from bituminous black coal) or brown (from brown lignite coal) hydrogen. Black or brown hydrogen - most environmentally damaging as both the CO₂ and CO are not recaptured.

Blue hydrogen: 85-95% carbon generated from steam reforming is captured and stored underground through industrial carbon capture and storage (CCS).

Turquoise hydrogen: refers to a way of creating hydrogen through a process called methane pyrolysis, which generates solid carbon. As such, there is no need for CCS.

<https://www.weforum.org/agenda/2021/07/clean-energy-green-hydrogen/>

Hydrogen Production Today: Fossil Fuel Reforming



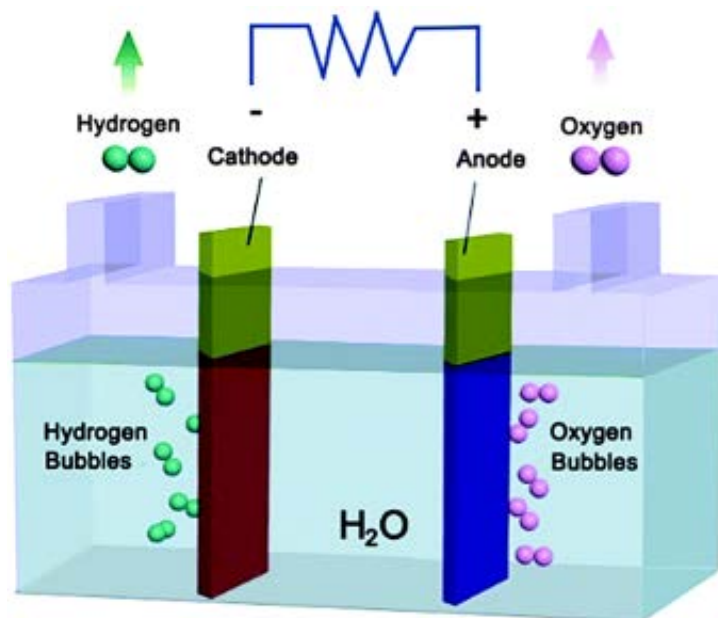
- Year 2022 global demand for hydrogen - 70 million metric tons,
- 99% of which comes from fossil fuels = 76% from natural gas + 23% from coal
- **<1% from the electrolysis of water**
- Current H_2 production consumes 6% of the global natural gas and 2% of the global coal
- This results in CO_2 emissions of around 830Mt/year out of which only 130Mt/year is being captured and used in the fertilizer industry.

Hydrogen Production Tomorrow: Splitting H₂O

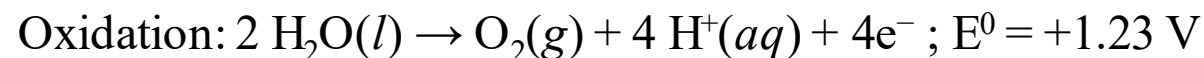
Electrolytic Processes

Water electrolysis uses electricity to split water into hydrogen and oxygen. Hydrogen produced via electrolysis can result in zero greenhouse gas emissions, depending on the source of the electricity used.

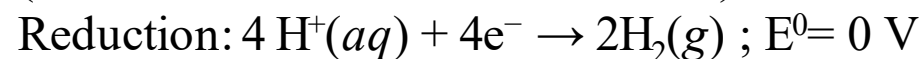
Water Electrolysis (Splitting Water Using Electricity)



At the positively charged anode, an **oxidation** reaction occurs. The electrons from water are given to the anode which move via the external circuit to the –ive cathode. The hydrogen cations move through the water to the –ive cathode.



At the negatively charged cathode, a **reduction** reaction takes place, with electrons (e^-) (coming from anode side through external ckt) being given to hydrogen cations (coming from anode through water) to form hydrogen gas (the half reaction balanced with acid)



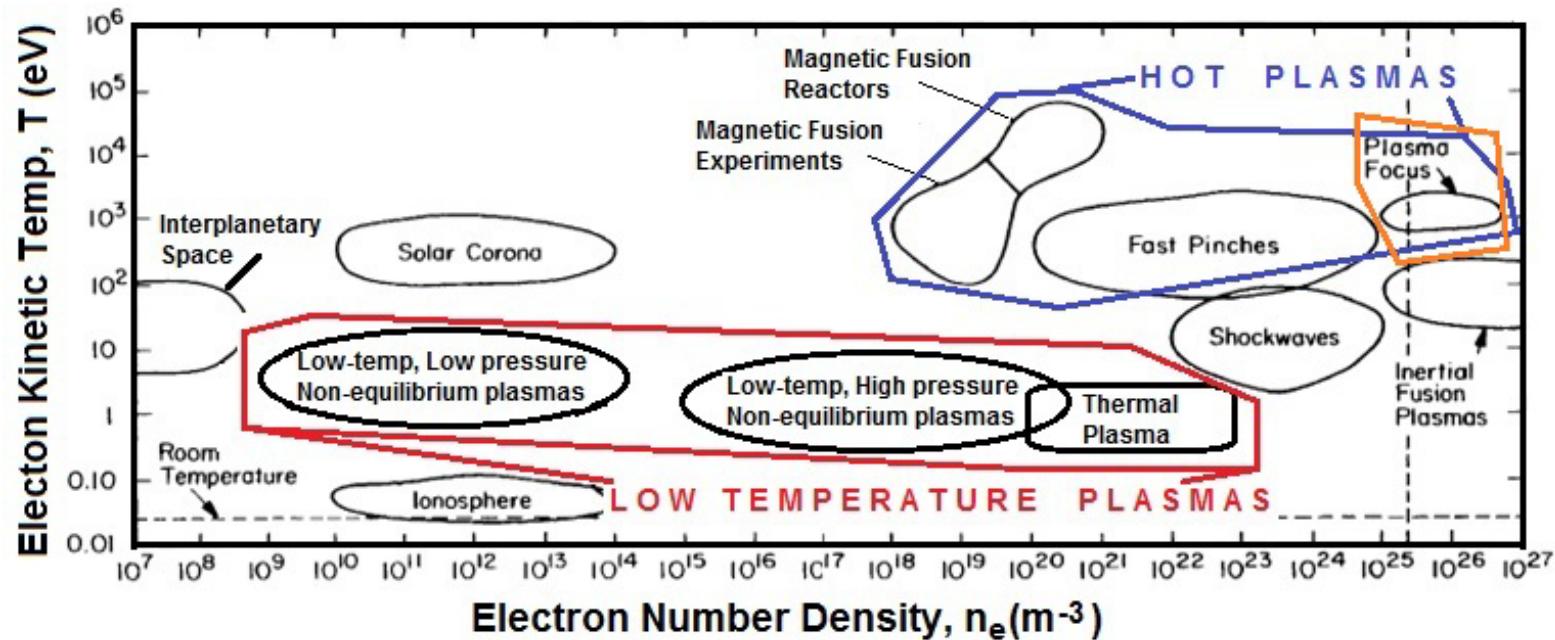
Thus, the standard potential of the water electrolysis cell ($E^0_{\text{cell}} = E^0_{\text{cathode}} - E^0_{\text{anode}}$) is -1.23 V at 25°C

ISSUES:

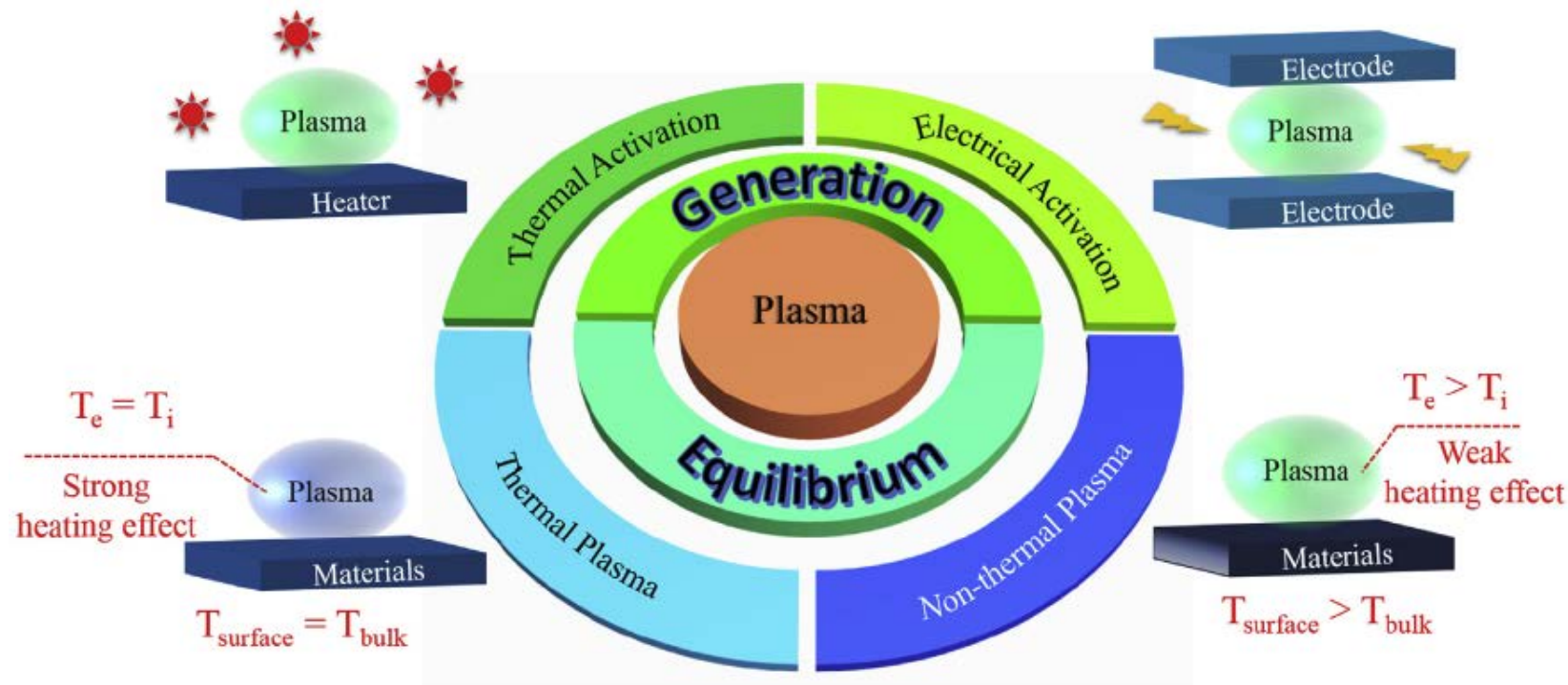
- **Overpotential** are needed for electrolysis - to overcome various obstacles such as the circuit resistance, electrolyte conductivity, surface transfer rate, patency of surface bubbles, and more importantly, the sluggish kinetic steps involved in OER and HER.
- Currently Pt is the best with lowest overpotential and very high stability
- Pt is expensive and rare
- **Non-noble metal with lower overpotential and higher stability are needed**

Plasma Type	Low -temp, Non-equilib., Low-pressure	Thermal Plasma	Low-temp, Non-equilib., High Pressure	High-pressure Microplasma	Plasmas in Liquids	High Energy Density Pinch Plasma
T_e	Few to tens of eV	0.1 – 5 eV	2 – 5 eV	> 10 eV	1 – 2 eV	200 – 2000 eV
N_e	$10^9 - 10^{14} \text{ m}^{-3}$	$10^{19} - 10^{23} \text{ m}^{-3}$	$10^{16} - 10^{20} \text{ m}^{-3}$	10^{18} m^{-3}	$10^{21} - 10^{23} \text{ m}^{-3}$	$10^{25} - 10^{26} \text{ m}^{-3}$
	Non-equilibrium	Equilibrium	Non-equilibrium	Non-equilibrium	Non-equilibrium	Non-equilibrium
K. Ostrikov et al. JPD:AP 44 (2011) 17400						Ion-beam Electron-beam Shock wave

Plasmas of Interest for Nanomaterials



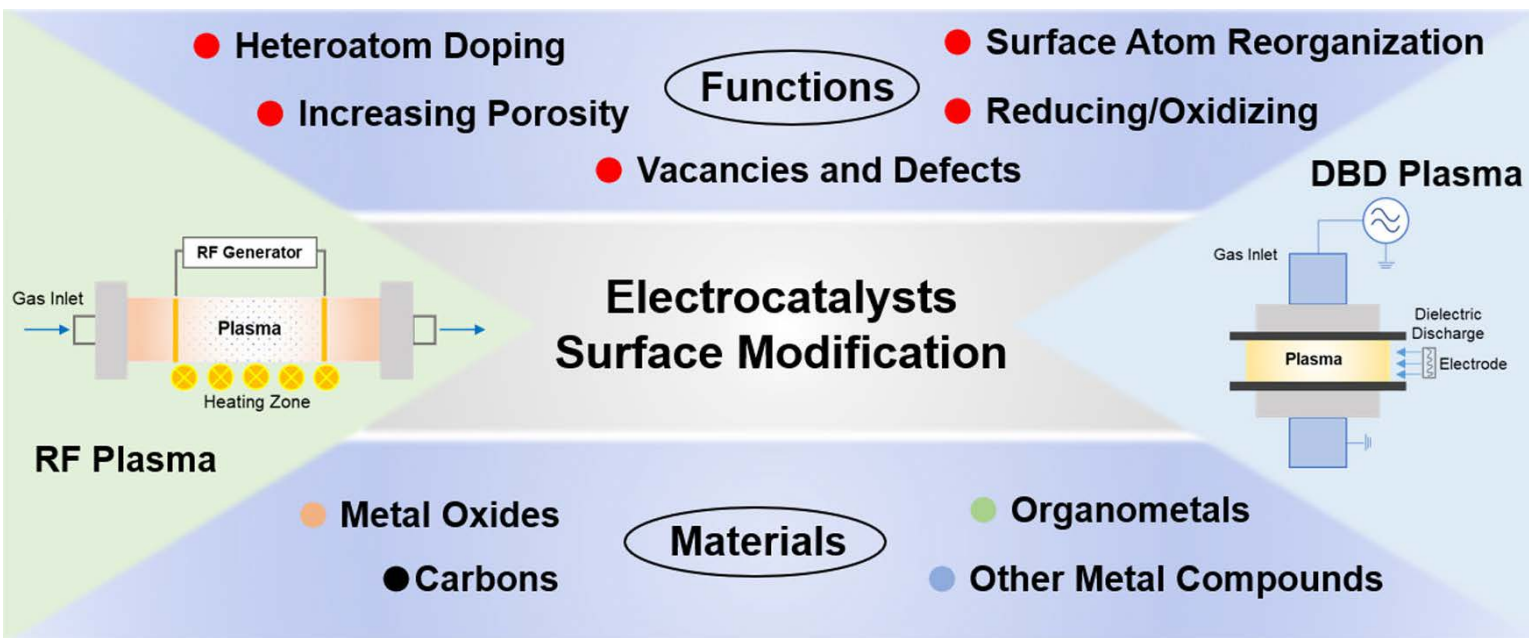
Plasmas for Materials



Thermal Plasma – due to extraordinary kinetic features of ions and electrons they not only shows highly reactive behavior but also exhibits considerably intense heating effect leading to melting and even vaporization of most materials. However, the heating effect is harmful to the fabrication of nanostructured materials.

Non-thermal Plasma (Cold Plasma) – has lesser or no heating effect but has high chemical activity. This unique property of cold plasma is very desirable for material processing, especially for those sluggish reactions or materials sensitive to heat → extensively studied in preparation of nanomaterials.

Effects of Plasmas on Electrocatalysts



J. Tang et al., *Energy Technologies* 2022, 10, 2200235

In non-equilibrium plasmas, the fast electrons act on different gas molecules to produce **the reactive species**, such as:

- excited atomic O, N, S, and P radicals,
- as well as molecular O_2^+ , N_2^+ , H_2^+ , NH_2^+ , and OH^- radicals under certain atmosphere composition and operating conditions.

Interactions between the electrocatalyst surface and plasma generated radicals **can bring various functions to the electrocatalyst**, such as:

- reorganizing surface atoms**,
 - Y. Hao, et al, *ACS Appl. Mater. Interfaces* 2020, 12, 29393;
 - K. Xu, et al, *Adv. Mater.* 2018, 30, 1703322;
 - X. Wang, et al. *Angew. Chem., Int. Ed.* 2018, 57, 16421.
 - introducing vacancies/defects**,
 - Y. Lu, et al. *ACS Sustain. Chem. Eng.* 2019, 7, 2906;
 - Y. Tian, et al., *Appl. Catal. A: General* 2017, 529, 127;
 - L. Tao, et al *Chem. Commun.* 2016, 52, 2764.
 - doping with heteroatoms**,
 - W. Zhong, et al., *J. Mater. Chem. A* 2017, 5, 16605;
 - L. Li, et al., *ACS Energy Lett.* 2017, 2, 294.
 - partially reducing or oxidizing surface, and**
 - H. Mistry, et al., *Nat. Commun.* 2016, 7, 12123.
 - enhancing the roughness and/or creating porosities**,
 - J. Zhou, et al., *Int. J. Hydrogen Energy* 2017, 42, 27004;
 - I. Kondratowicz, et al., *Appl. Surf. Sci.* 2018, 440, 651.
- to favor the electrocatalysis activity of the material.

Advantages of Non-thermal Plasmas for fabrication and modification of Electrode Materials

- Firstly, the presence of excited species in plasma results in an **intrinsically high chemical reactivity even at ambient temperature**. High reactivity leads to three typical consequences:
 - **high-surface selectivity during processing**
[M. Schaepkens et al., J. Vac. Sci. Technol. A 17 (1999) 26-37],
 - **desirable production efficiency**
[M. Moreau et al., Biotechnol. Adv. 26 (2008) 610-617], and
 - **broad selection of starting materials**
[D.H. Seo et al., Adv. Energy Mater. 3 (2013) 1316-1323]
- Secondly, little heating effect is present in non-thermal plasmas, which is favorable for the **preservation of nano-framework**
 - [T. Desmet et al., Biomacromolecules 10 (2009) 2351-2378]
 - [R.A. Surmenev et al., Surf. Coat. Technol. 206 (2012) 2035-2056]

Mechanism of Plasma-induced Surface Modification of Electrocatalyst Materials

Plasma-generated excited species can interact with the first few atomic layers on the material thus results in physical and/or chemical modification of the material surface, while maintaining the properties of the bulk.

Plasma processing mainly tunes the surface properties of the electrocatalyst material by the following mechanisms:

- 1) The excited radical species can react with materials surface to form new chemical bonds, resulting in new doping functionalities.
- 2) The high energy radicals in plasma could attack the material surface to subsequently exfoliating or engraving the material surface to increase roughness and porosity.
- 3) The redox ions generated in plasma can partially reduce or oxidize the material surface to tune the electronic properties of the active sites.

Using Carbon Plasmas

1. B. Ouyang, Y. Wang, X. Wang, Z. Zhang, F. Liu, Z. Fang, E. Kan, and **R. S. Rawat***, *Rational design of hierarchically structured dual-encapsulated CoMoO₄ nanosheets via in situ plasma tuning for efficient Li⁺ storage*, MRS Bulletin 47 (7), 656-664 (2022). – **IF: 6.578**
2. B. Ouyang, D. L. Chao, G. C. Jia, Z. Zhang, E. Kan, H. J. Fan and **R. S. Rawat***, *C-Plasma Derived Precise Volumetric Buffering for High-Rate and Stable Alloying-Type Energy Storage*, Nano Energy 80, 105557 (2021). – **IF: 16.602**
3. B. Ouyang, D. L. Chao, G. C. Jia, Z. Zhang, H. J. Fan and **R. S. Rawat***, *Hierarchical vertical graphene nanotube arrays via universal carbon plasma processing strategy: A platform for high-rate performance battery electrodes*, Energy Storage Materials 18, 462-469 (2019). – **IF: 16.42**
4. Dongliang Chao, Bo Ouyang, Pei Liang, Tran Thi Thu Huong, Guichong Jia, Hui Huang, Xinhui Xia, **Rajdeep Singh Rawat***, and Hong Jin Fan*, *C-Plasma of Hierarchical Graphene Survives SnS Bundles for Ultra-Stable and High Volumetric Na-Ion Storage*, Advanced Materials 1804833 (2018). - **IF: 30.85**
5. Yongqi Zhang, Bo Ouyang, Zheng Zhang, **R. S. Rawat***, and Hong Jin Fan, *Pre-reduction of Metal Oxides via Carbon Plasma Treatment for Efficient and Stable Electrocatalytic Hydrogen Evolution*, Small, 1800340 (2018). - **IF: 15.15**
6. Mohan V. Jacob*, Dai Taguchi, Mitsumasa Iwamoto, Kateryna Bazakaa, and **Rajdeep Singh Rawat**, *Resistive switching in graphene–organic device: Charge transport properties of graphene-organic device through electric field induced optical second harmonic generation and charge modulation spectroscopy*, Carbon 112, 111-116 (2017). **IF: 9.59**
7. Yongqi Zhang, Guichong Jia, Huanwen Wang, Bo Ouyang, **Rajdeep Singh Rawat**, and Hong Jin Fan*, *Ultrathin CNTs@FeOOH nanoflakes core/shell networks as efficient electrocatalysts for oxygen evolution reaction*, Materials Chemistry Frontiers 1, 709-715 (2017). - **IF: 6.48**
8. Bo Ouyang, Yongqi Zhang, Zheng Zhang, Hong Jin Fan and **R.S. Rawat***, *Green synthesis of vertical graphene nanosheets and their application in high-performance supercapacitors*, RSC Advances 6, 23968-23973 (2016): - **IF: 3.36**
9. Bo Ouyang, Ying Wang, Zheng Zhang, and **R.S. Rawat***, *MoS₂ anchored free-standing three dimensional vertical graphene foam based binder-free electrodes for enhanced lithium-ion storage*, Electrochimica Acta 194, 151-160 (2016): **IF: 6.22**
10. Bo Ouyang, M.V. Jacob, and **R.S. Rawat***, *Free standing 3D graphene nano-mesh synthesis by RF plasma CVD using non-synthetic precursor*, Material Research Bulletin 71, 61-66 (2015): **IF: 4.64**
11. M.V. Jacob, **R.S. Rawat**, Bo Ouyang, K. Bazaka, D. Sakthi Kumar, Dai Taguchi, Mitsumasa Iwamoto, Ram Neupane, and Oomman K. Varghese, *Catalyst-Free Plasma Enhanced Growth of Graphene from Sustainable Sources*, Nano Letters 15 (9), 5702–5708 (2015). **IF: 11.19**

Using Nitrogen Plasmas

1. Bo Ouyang, Chao Sun, Xi Wang, Jing Xu, Yanqiang Cao, Fan Wu, **Rajdeep Singh Rawat***, Jipeng Zhu, Erjun Kan*, *Structural control of heterostructured Co₃N-Co nano-corals for boosting electrocatalytic hydrogen evolution based on insulator-confined plasma engineering*, Chemical Engineering 466(15), 143211 (2023)
2. Bo Ouyang, Yongqi Zhang, X. Wang, Y. Deng, F. Liu, Z. Fang, **Rajdeep Singh Rawat***, and E. Kan*, *Facet control of Nickel nitride for efficient control of hydrogen evolution electrocatalysis via auxiliary cooling assisting plasma engineering*, Small 13, 2204634 (2022). **IF: 15.15**
3. W. Y. Lin, T. Li, L Akasyah, J. W. M. Lim, H. Xu, X. Py, **R. S. Rawat**, and A Romagnoli, *Comparison of sintering condition and radio frequency plasma discharge on the conversion of coal/biomass fly ash into high-temperature thermal energy storage material*, Energy Conversion and Management 192, 180 (2019). – **IF: 9.71**
4. Bo Ouyang, Yongqi Zhang, Zheng Zhang, Hong Jin Fan*, **Rajdeep Singh Rawat***, *Nitrogen-Plasma-Activated Hierarchical Nickel Nitride Nanocorals for Energy Applications*, Small 13(34), 1604265 (2017). **IF: 13.28**
5. Zhang Yongqi, **R. S. Rawat**, Fan Hongjin, *Plasma for rapid conversion reaction and surface modification of electrode materials*, Small Methods, 1(9), 1700164 (2017). – **IF: 14.19**
6. Bo Ouyang, Yongqi Zhang, Ying Wang, Zheng Zhang, Hong Jin Fan*, and **Rajdeep Singh Rawat***, *Plasma surface functionalization induces nanostructure and nitrogen-doping in carbon cloth with enhanced energy storage performance*, Journal of Material Chemistry A 4, 17801–17808 (2016). **IF: 12.73**
7. Y. Zhang, Bo Ouyang, J. Xu, G. Jian, S. Chen, **R. S. Rawat** and Hong Jin Fan*, *Rapid synthesis of cobalt nitride nanowire: Highly efficient and low-cost Catalysts for OER*, Andewandte Chemie Int. Ed. 55, 8670 (2016). **IF: 15.34 - WOS Highly Cited paper - 627**
8. Y. Zhang, Bo Ouyang, J. Xu, S. Chen, **R. S. Rawat*** and Hong Jin Fan*, *3D Porous Hierarchical Nickel-Molybdenum Nitrides Synthesized by RF Plasma as Highly Active and Stable Hydrogen Evolution Reaction Electrocatalysts*, Advanced Energy Materials 6, 1600221 (2016). – **IF: 29.37 - WOS Highly Cited paper - 434**

Outline of Presentation

Introduction – Energy Conversion and Plasmas,

- Hydrogen Economy (Energy Conversion)
- Our focus - plasma based strategies
- Plasma processing/depositions for EC-Energy conversion/storage Materials

Some examples of application of low temperature nitrogen/carbon plasmas for energy Conversion applications

Major focus - Facet Control of Ni_3N Nano-Framework for Efficient HER via Auxiliary Cooling Assisted Plasma Engineering

Conclusions

Example 1: TMNs for Hydrogen Evolution Reaction (HER)

- Exorbitant prices and low reserves of Pt electrocatalysts → fabrication of highly efficient and stable non-precious metal-based electrocatalysts → typically transition metal nitrides (TMNs).^[1]
- Although recent studies on TMNs nano-frameworks ($\text{Ni}_3\text{N}/\text{Ni}$,^[2] NiMoN ^[3] and NiFeMoN ^[4]) have confirmed them to be efficient HER electrocatalysts, but complicated fabrication procedures with considerable energy consumption, especially **thermal nitridation**, inevitably deteriorates nanostructures, leading to the restriction of their broad application.
- Consequently, cold plasma strategy has received tremendous interests in fabricating various TMN nanostructures for further improving their HER performances.^[5, 6] Typically, we have synthesized highly purified Ni_3N , CoN and NiMoN nano-structured electrodes for enhanced electrocatalytic activities based on direct N_2 plasma nitridation of the corresponding metallic sources.^[7, 8]

1. J. Xie, Y. Xie, *Chem. Eur. J.* **2016**, *22*, 3588-3598.

2. F. Song, W. Li, J. Yang, G. Han, P. Liao, Y. Sun, *Nat. Commun.* **2018**, *9*, 4531.

3. B. Chang, J. Yang, Y. Shao, L. Zhang, W. Fan, B. Huang, Y. Wu, X. Hao, *ChemSusChem* **2018**, *11*, 3198-3207.

4. C. Zhu, Z. Yin, W. Lai, Y. Sun, L. Liu, X. Zhang, Y. Chen, S.-L. Chou, *Adv. Energy Mater.* **2018**, *8*, 1802327.

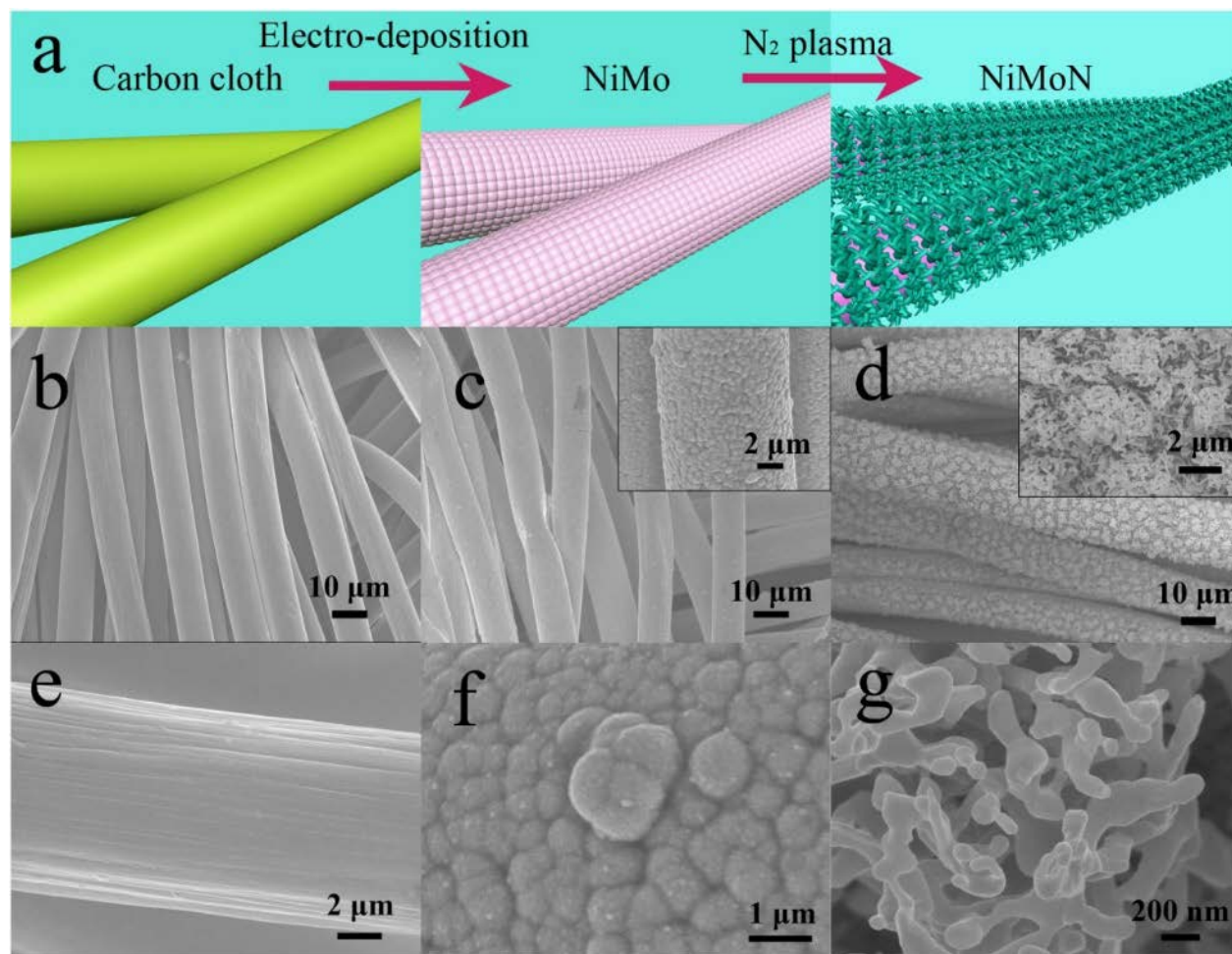
5. B. Ouyang, Y. Zhang, X. Xia, R. S. Rawat, H. J. Fan, *Mater. Today Nano* **2018**, *3*, 28-47.

6. J. Sun, D. Alam, R. Daiyan, H. Masood, T. Zhang, R. Zhou, P. J. Cullen, E. C. Lovell, A. Jalili, R. Amal, *Energy Environ. Sci.* **2021**, *14*, 865-872.

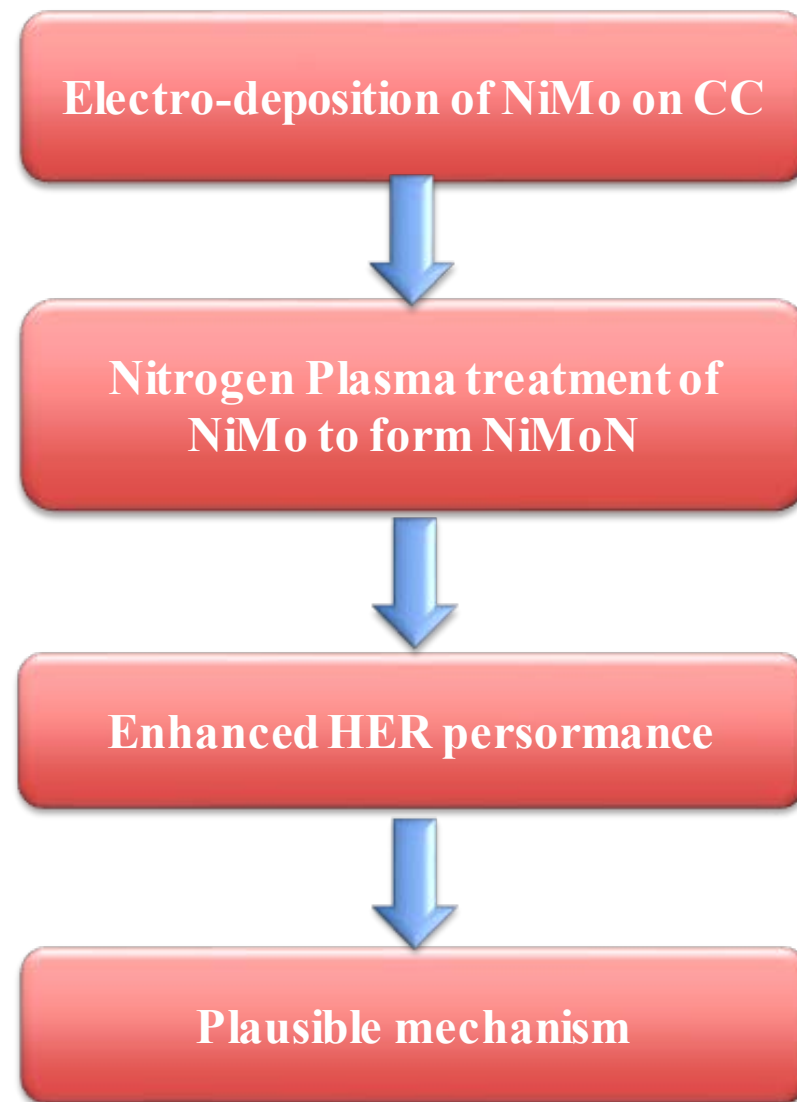
7. B. Ouyang, Y. Zhang, Z. Zhang, H. J. Fan, R. S. Rawat, *Small*, **2017**, *13*, 1604265.

8. Y. Zhang, B. Ouyang, J. Xu, S. Chen, R. S. Rawat, H. J. Fan, *Adv. Energy Mater.* **2016**, *6*, 1600221.

Example 1: 3D hierarchical porous NiMoN for highly active and stable Hydrogen Evolution Reaction

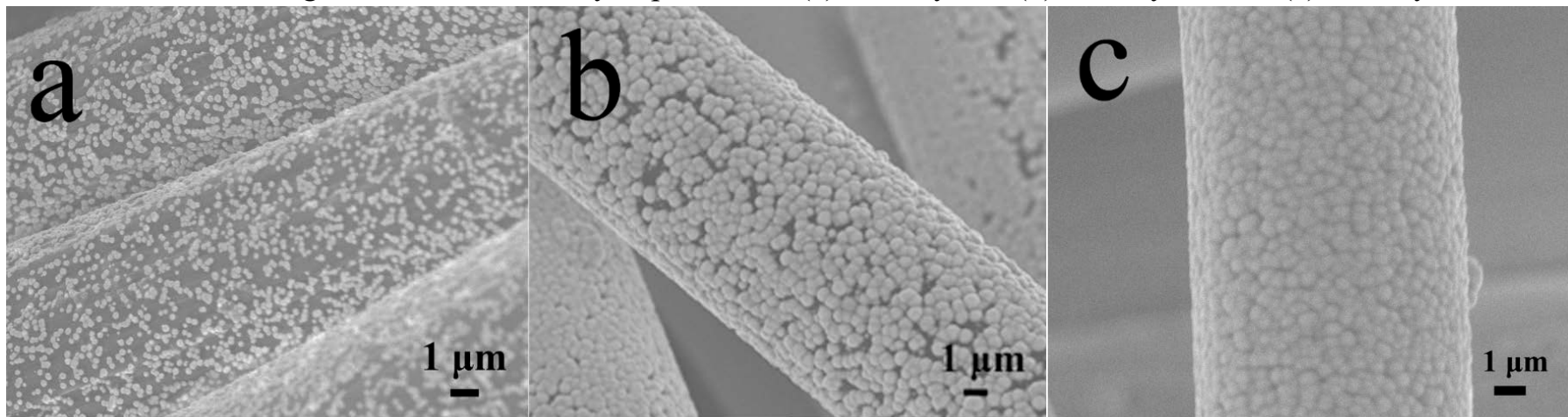


3D hierarchical porous nickel molybdenum nitride (NiMoN). SEM images of (b, e) carbon cloth, (c, f) NiMo alloy deposited for 7200 cycles and (d, g) NiMoN treated under N₂ plasma for 15 min.

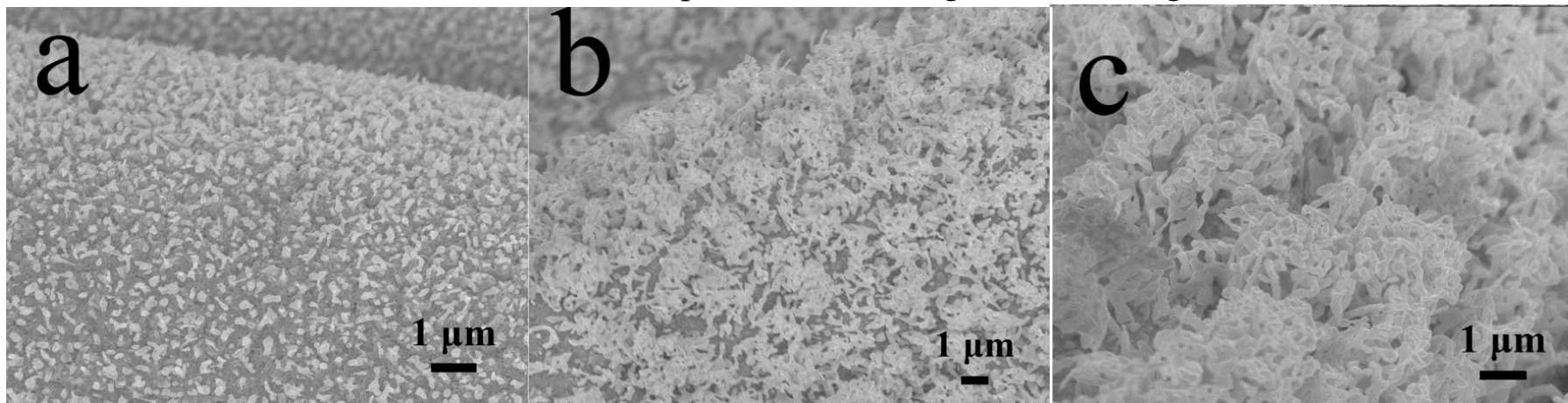


Example 1: Nitrogen functionalization and Nanostructurization of NiMo to NiMoN

SEM images of PED NiMo alloy deposited for (a) 1800 cycles, (b) 3600 cycles and (c) 7200 cycles

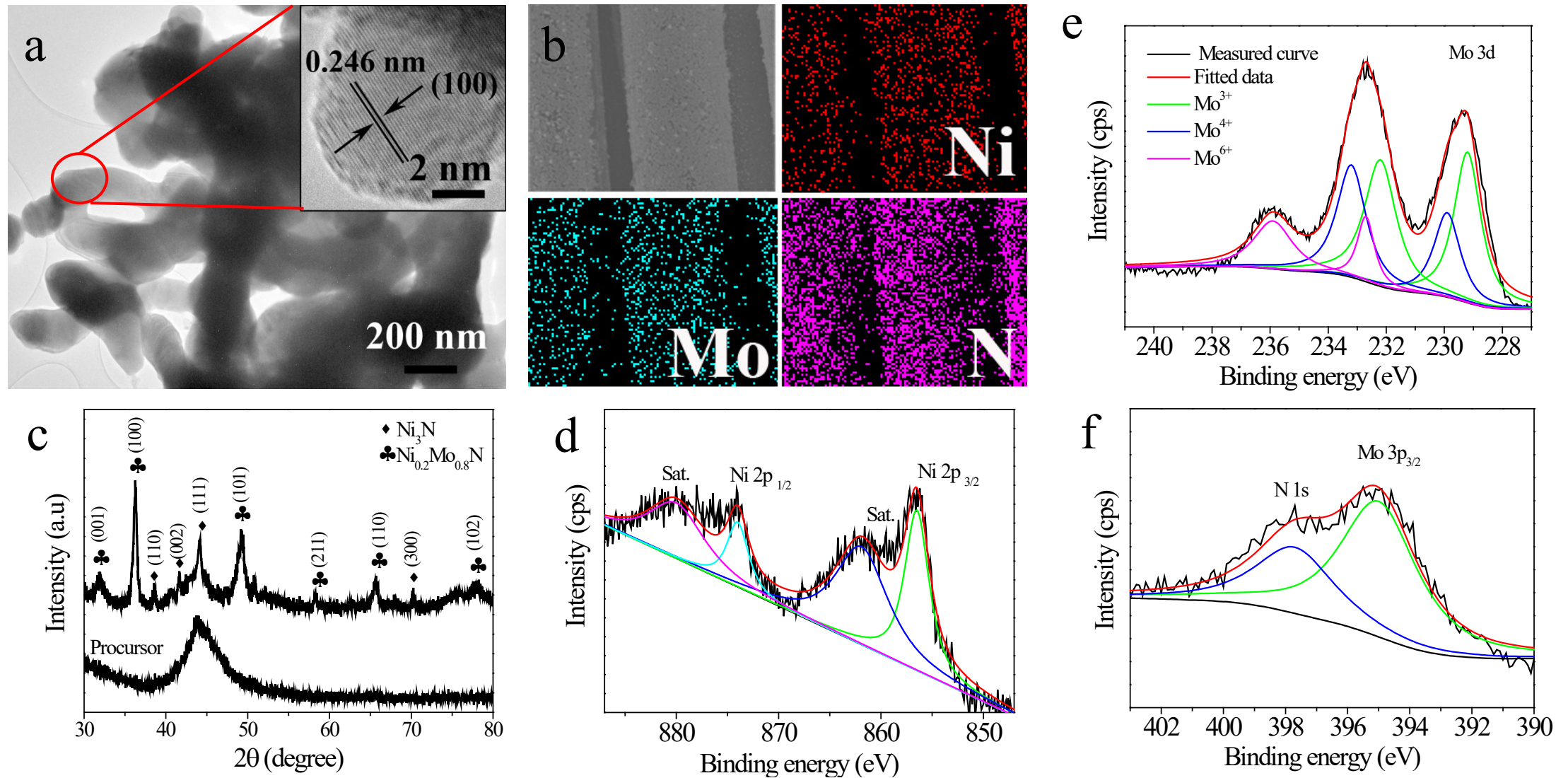


PECVD Chamber (i) pressure 0.2 mbar under nitrogen flow (100 sccm), (ii) temperature of chamber 450 °C, (iii) RF-plasma power 250 W at 13.56 MHz for 15 min. After the RF plasma, the average mass loading decreased to around 1.1 mg cm².



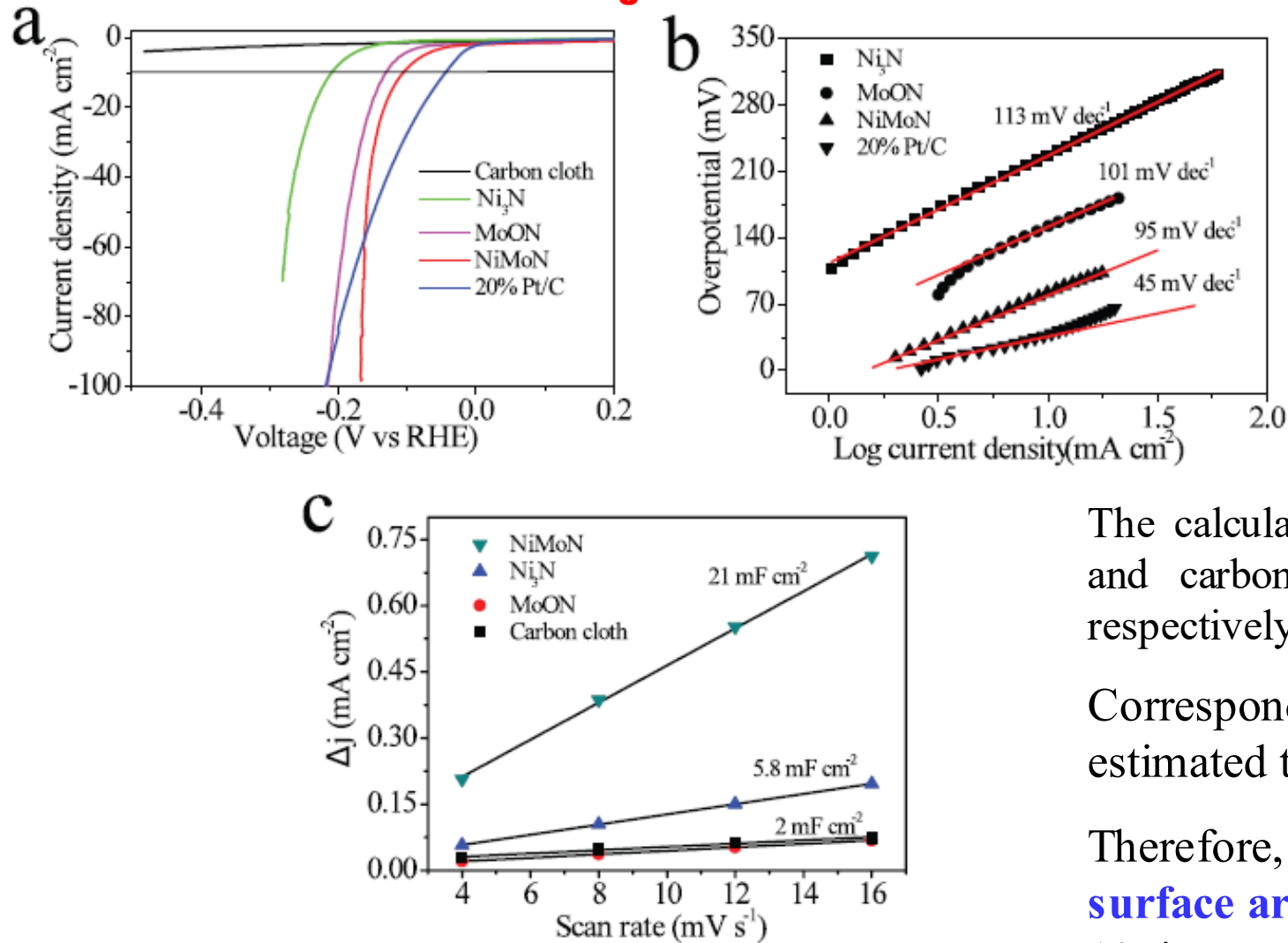
SEM images of NiMo alloy at different N₂ plasma activation duration (a) 5 min, (b) 10 min and (c) 15 min

Example 1: Nitrogen functionalization and Nanostructurization of NiMo to NiMoN



Structural and composition characterization of NiMoN: (a) TEM image of NiMoN, inset of (a) is HRTEM image, (b) Elemental maps of Ni, Mo and N. (c) XRD patterns; XPS spectra of (d) Ni 2p, (e) Mo 3d and (f) N 1s-Mo 3p.

Example 1: Catalytic Properties of NiMoN, Ni₃N, MoON, and carbon cloth



The calculated **capacitances** of NiMoN, MoON, Ni₃N, and carbon cloth are 21, 2, 5.8, and 2 mF cm⁻², respectively.

Correspondingly, **the roughness factors** are estimated to be around 1050, 100, 290, and 100.

Therefore, the NiMoN electrode has an **active surface area** 3.6 times that of the Ni₃N and almost 10 times of MoON and carbon cloth.

a) Polarization curves, (b) Tafel slopes, and

(c) current density as a function of scan rate of various catalysts

Example 1: Comparative performance of NiMoN, Ni₃N, MoON, and carbon cloth

Table 1. Properties of various catalysts.

	$\eta_{\text{onset}}[\text{mV}]$	$\eta_{10}[\text{mV}]$	Tafel slope [mV dec ⁻¹]	Exchange current j_0 [mA cm ⁻²]
Ni ₃ N	161	208	113	0.12
MoON	95	146	101	0.22
NiMoN	50	109	95	0.92
20% Pt/C	0	43	45	0.72

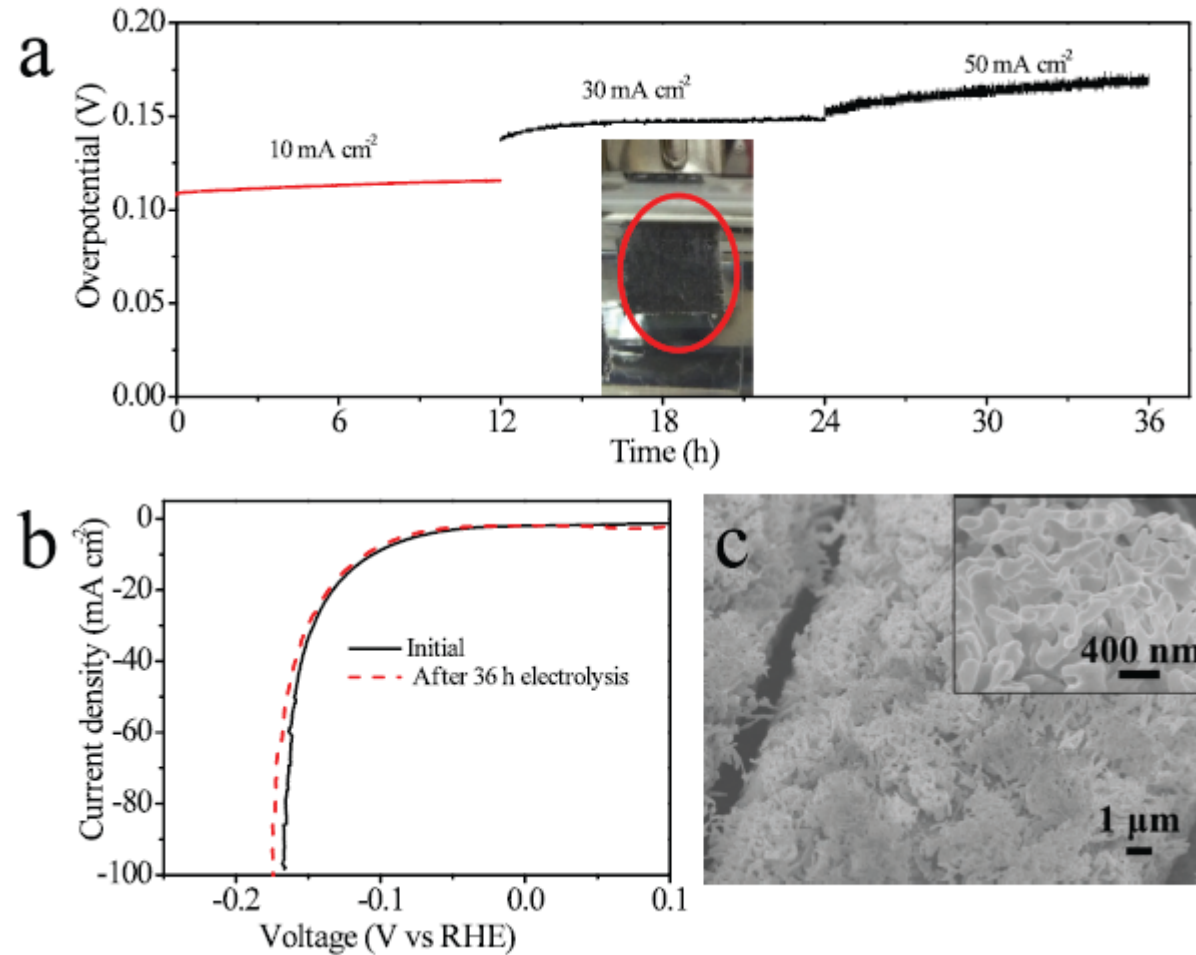
Table 2. Charge-transfer impedances at different overpotentials for various catalysts.

	$R_{\text{ct}}[\Omega]$		
	$\eta_{\text{onset}}-50 \text{ mV}$	η_{onset}	$\eta_{\text{onset}}+50 \text{ mV}$
Ni ₃ N	596	123	52.5
MoON	625	149	30.5
NiMoN	302.4	55	26.4

The **small** Tafel slope value and **high** exchange current density **demonstrate the superior HER activity**; which implies NiMoN has best HER activity among various catalysts investigated in this study.

With increase of overpotential (η), the values of charge transfer impedance R_{ct} for all catalysts decrease quickly. **NiMoN presents the smallest R_{ct} (55 Ω) at onset potential** compared to that of MoON (149 Ω) and Ni₃N (123 Ω) => **highly active HER kinetics**

Example 1: Stability of Catalytic Performance of NiMoN



a) Stability tests of the NiMoN electrode at current densities of 10, 30, and 50 mA cm⁻² over 36 h (the inset photograph shows the bubble generation at 30 mA cm⁻²). b) Polarization curves before and after 36 h stability test. c) SEM image of the electrode surface after 36 h electrolysis.

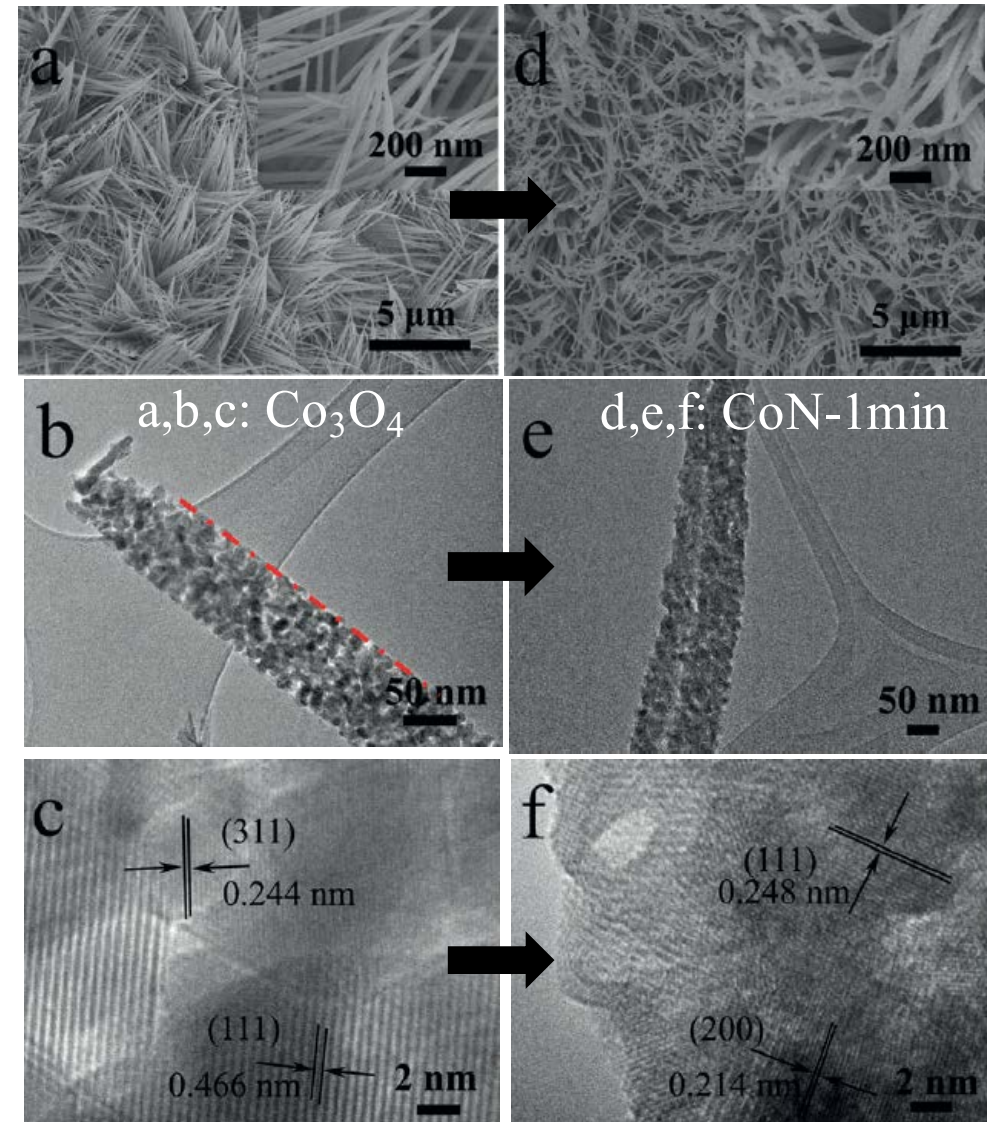
Example 2: Rapid Synthesis of Cobalt Nitride Nanowires: Highly Efficient & Low-Cost Catalysts for O₂ Evolution

Aim: Develop efficient, durable, and earth-abundant electrocatalysts **for the oxygen evolution reaction (OER)** by water splitting

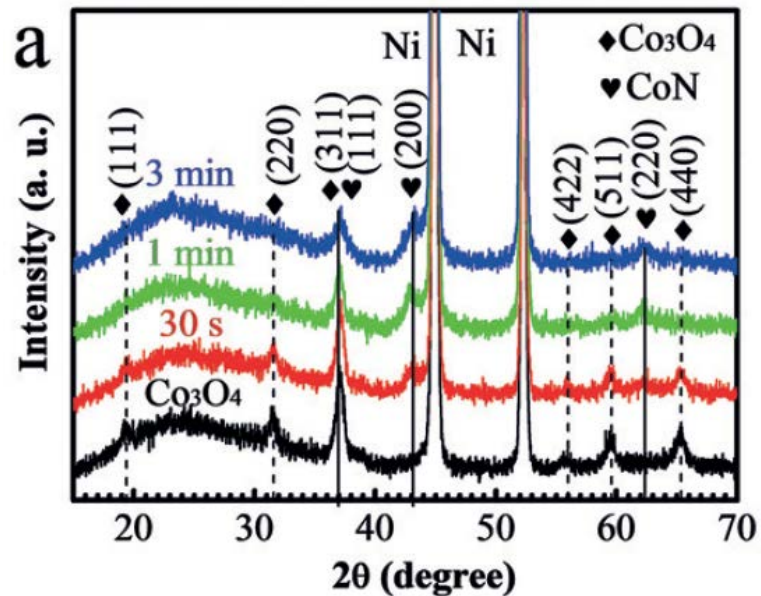
How: By rapid synthesis of transition-metal nitride nanostructures using nitrogen plasma treatment **to convert cobalt oxide precursors into cobalt nitride nanowires.**

Advantages: Requires **significantly shorter reaction times (about 1 min)** at **room temperature** compared to conventional high-temperature NH₃ annealing which requires a few hours.

Significantly enhances the OER activity, as evidenced by a low overpotential of 290 mV to reach a current density of 10 mA cm⁻², a small Tafel slope, and long-term durability in an alkaline electrolyte.

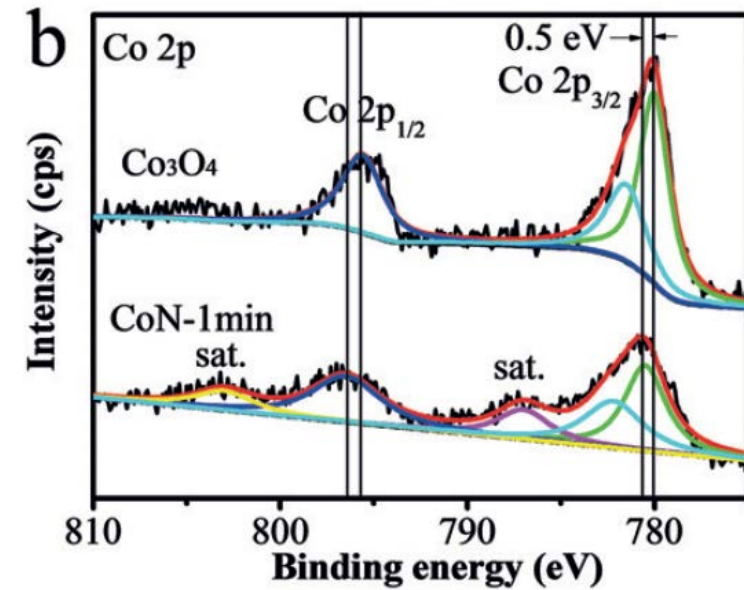


Example 2: Co_3O_4 to complete CoN Transformation by nitrogen plasma treatment



XRD patterns of Co_3O_4 , CoN-30 s, CoN-1 min, and CoN-3 min. The dashed and solid lines indicate the peak positions of Co_3O_4 and CoN, respectively.

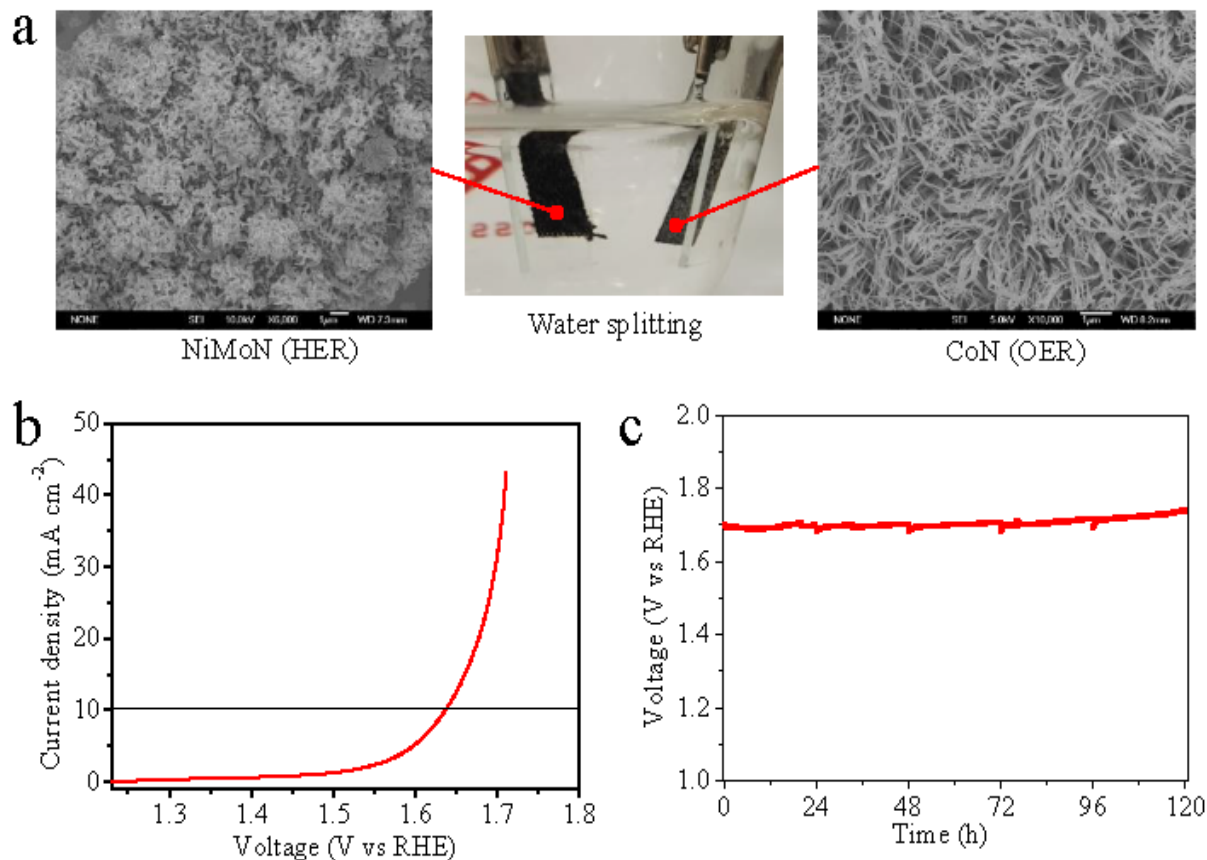
- For CoN-30s sample, peaks for Co_3O_4 and CoN coexist. The peak attributed to the (311) plane of Co_3O_4 and (the 111) plane of CoN overlap at 36.5–36.88.
- For the CoN-1min sample, only peaks indexed to CoN remain (solid line).
- No difference between the patterns of CoN-3min and CoN-1min, implying that pure CoN nanowire arrays were obtained after just 1 min of N_2 plasma treatment.



XPS $\text{Co}2p$ spectra of Co_3O_4 and CoN-1 min

- Relatively weak satellite peaks in Co_3O_4 spectra confirms its characteristic spinel structure, with Co^{3+} cations occupying octahedral lattice sites and Co^{2+} cations in tetrahedral sites.
- The emergence of well-defined satellite peaks (at 787.3 and about 803.2 eV) in the CoN-1 min sample is consistent with the breakdown of the spinel structure.
- Both peaks of the CoN-1min sample show a positive chemical shift by 0.5 eV compared with that of Co_3O_4 , indicating a modulation of the surface electronic band bending after N_2 plasma.

Example 2: Overall Water Splitting of NiMoN || CoN Electrolyzer Cell



Overall water splitting. NiMoN nanodendrite is the HER electrode and CoN nanowire is the OER electrode. (a) The iR-corrected polarization curve of water electrolysis at a scan rate of 5 mV s⁻¹. (b) Stability test at 30 mA cm⁻² for 120 h.

Porous NiMoN was synthesized by N₂ plasma treatment of NiMo alloy, and exhibited efficient HER activity achieving a current density of 10 mAcm⁻² at an overpotential as low as 109 mV.

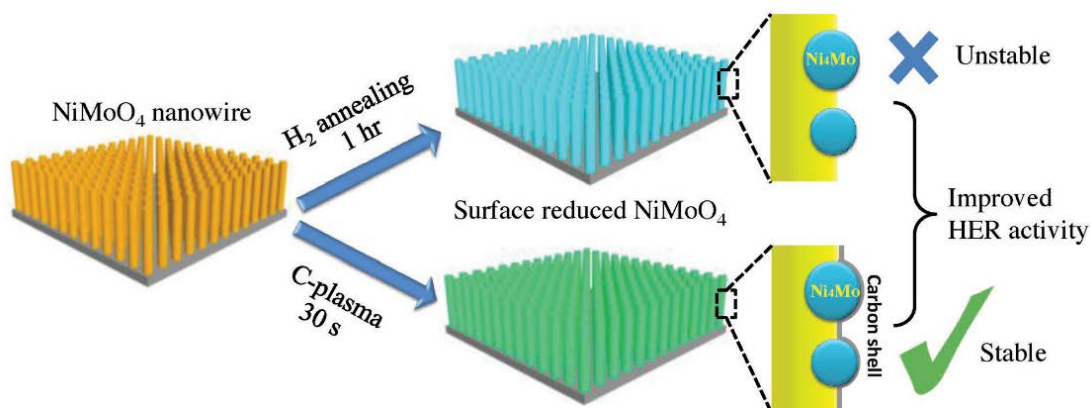
The NiMoN||CoN electrolyzer cell affords a current density of 10 mAcm⁻² at the operating potential of 1.63 V, representing a combined overpotential of 400 mV for overall water splitting.

This voltage is comparable to that of previously reported electrocatalysts.

More importantly, this combined electrolyzer cell exhibited an excellent stability: the operating voltage remained stable at around 1.7 V at a fixed current density of 30 mAcm⁻² for 120h of continuous electrolysis.

Example 3: Prereduction of MO by Carbon Plasma for Efficient and Stable Hydrogen Evolution Reaction (HER)

- **TMOs** – Advantages: easily available; variety of nanostructural form; and high SSA
- **Limitations of TMOs** – they fail for HER due to their low electrical conductivity, sluggish catalytic kinetics, and poor long term stability → improvement is highly desirable
- Li et al [Nat. Commun. 2015, 6, 8064] → commercial WO_3 nanoparticles can show enhanced HER activity after annealing under H_2 atmosphere
- We found [Small 2018, 1800340] that TMOs (NiMoO_4 , Co_3O_4 , and NiO) show a **self-activation** during the continuous HER process → due to the surface reduction of TMOs by the highly active hydrogen produced on their surface during HER process.
- **In situ improvement by self-activation** is slow (few hours), transient, and extremely unstable; the catalytic activity degrades quickly when the H_2 evolution is interrupted.
- So **prereduction of metal oxides** should be a more feasible and efficient strategy



High temp and long annealing time **may destroy the nanostructure**; and also the reduction is unstable → degradation of HER activity

Yongqi Zhang, Bo Ouyang, Zheng Zhang, R. S. Rawat, and Hong Jin Fan, *Pre-reduction of Metal Oxides via Carbon Plasma Treatment for Efficient and Stable Electrocatalytic Hydrogen Evolution*, Small, 1800340 (2018). **IF: 13.28**

Example 3: Prereduction of MO by Carbon Plasma for Efficient and Stable HER

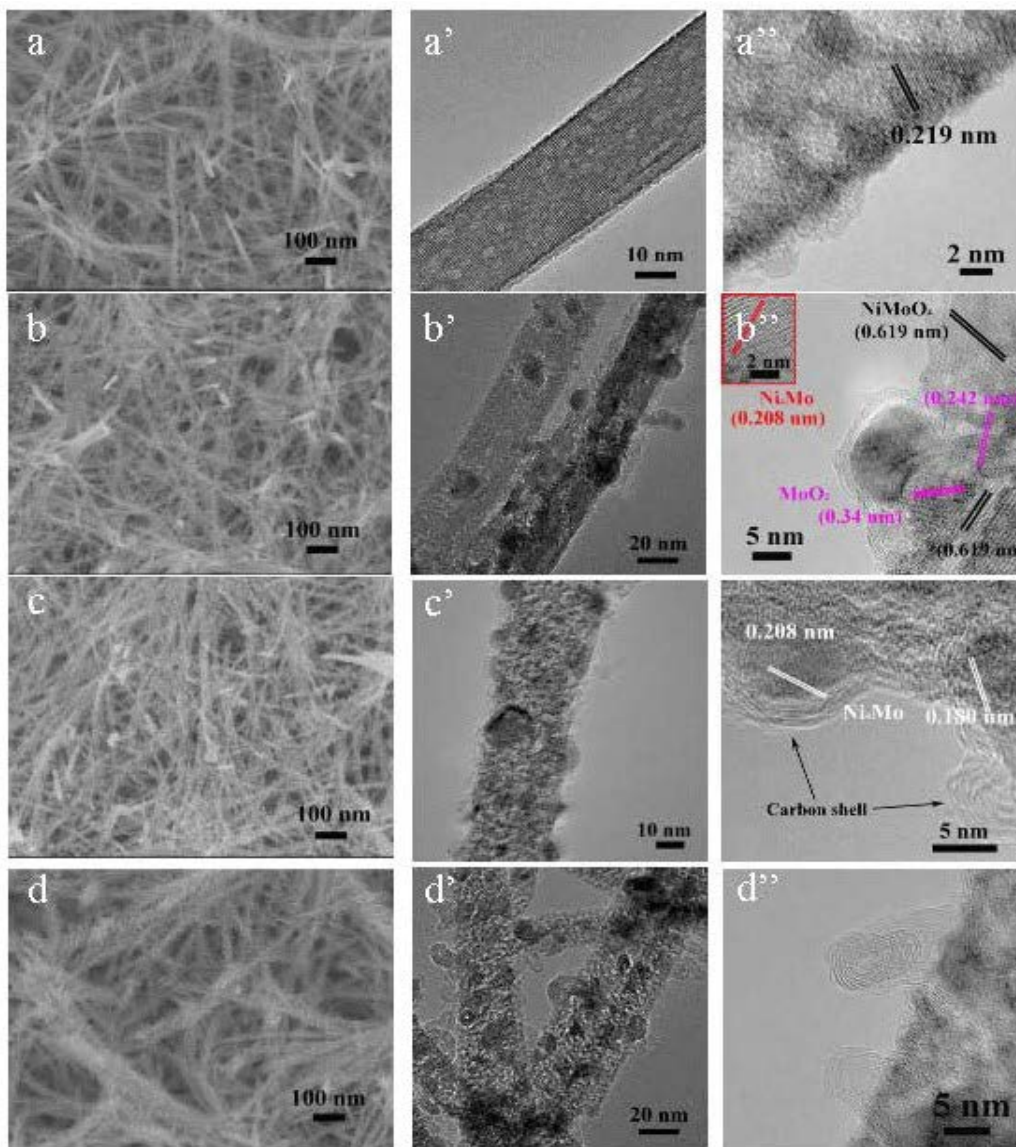
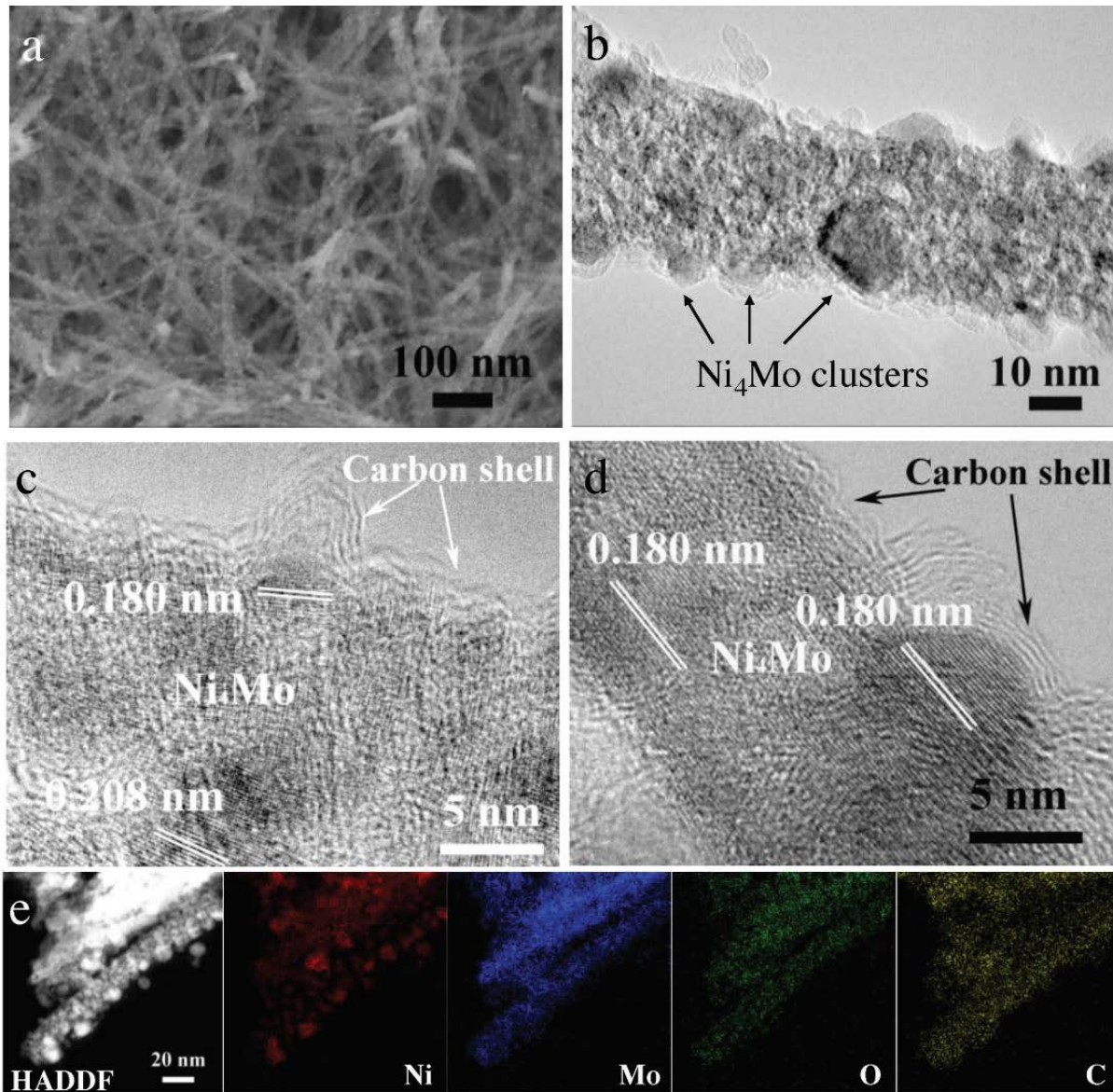


Figure S2. SEM and TEM images of the NiMoO_4 nanowires before and after C-plasma treatment for different time: a) no treatment, b) C-15s, c) C-30s and d) C-60s.

- NiMoO_4 NW arrays on CC by salvothermal
- **C-plasma treatment** \rightarrow active species of Ni_4Mo nanoparticles are produced due to reduction of the NiMoO_4
- NW array structure is well preserved due to a very short process time (15-30 s).
- Carbon shell is deposited on the nanowire surface \rightarrow chemical stability by preventing oxidation.
- Benefiting from highly exposed surface active sites (nanowire array), active Ni–Mo alloy NP decoration and protection by carbon shell, the C-plasma treated NiMoO_4 NW electrode displayed a low overpotential of 76 mV to reach 10 mA cm^{-2} in 1 m KOH.
- This strategy is universal and also effective for Co_3O_4 nanowire arrays.

Example 3: Prereduction of MO by Carbon Plasma for Efficient and Stable HER



- NW array morphology preserved – Fig a
- 5–10 nm NPs decorate NWs - Fig b
- TEM images (Fig c,d) - d -spacing of 0.208 and 0.180 nm for NPs corresponding to the (121) and (310) plane of the **Ni_4Mo alloy**.
- **About 1–2 layers of carbon** were coated on the surface of NWs.
- High-angle annular dark-filed (HADDF) STEM image further confirmed metal NPs decorated NWs (Fig e).
- TEM EDX mappings - **homogenous distribution of Mo, O, and C throughout NWs**, while the Ni element was distributed granularly on the surface with distinguishable particle boundaries.

Example 3: Prerduction of MO by Carbon Plasma for Efficient and Stable HER

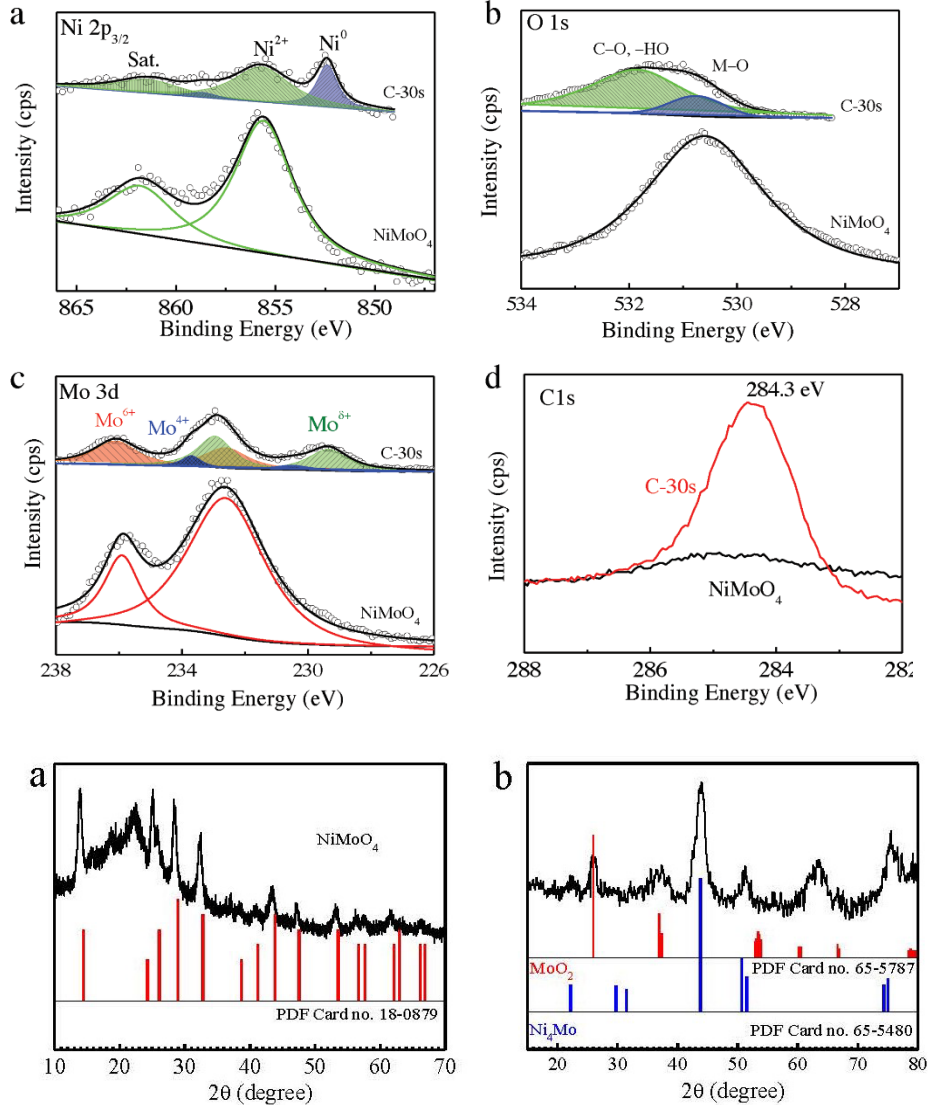


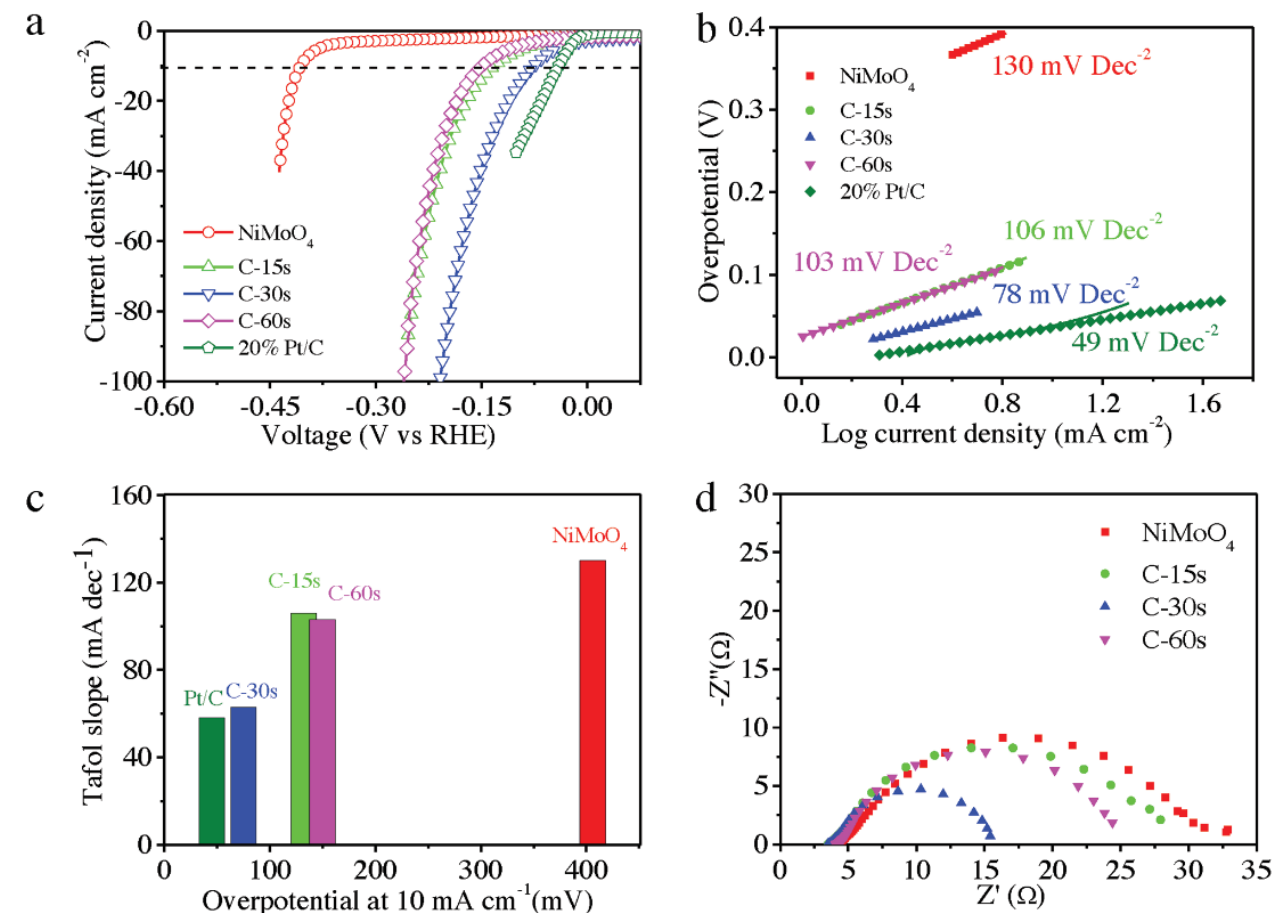
Fig S4. The powder XRD patterns of a) NiMoO₄ and b) C-30s

XPS confirm reduction by C-Plasma

- Fig a - After 30 s C-plasma treatment, **metallic Ni⁰ is observed** → reduction by carbon plasma
- Fig b - Intensity of 530.7 eV O 1s peak of O²⁻ ions in NiMoO₄ decreased for the C-30s sample and a new peak from the surface groups of carbon shell appeared at 531.8 eV → reduction by carbon plasma
- Fig c - Mo 3d spectra shows new peak at low BE of 229.4 eV after C-plasma treatment, which attributes to low valence Mo^{δ+} species ($\delta = 0, 1, 2, 3$) → reduction by carbon plasma

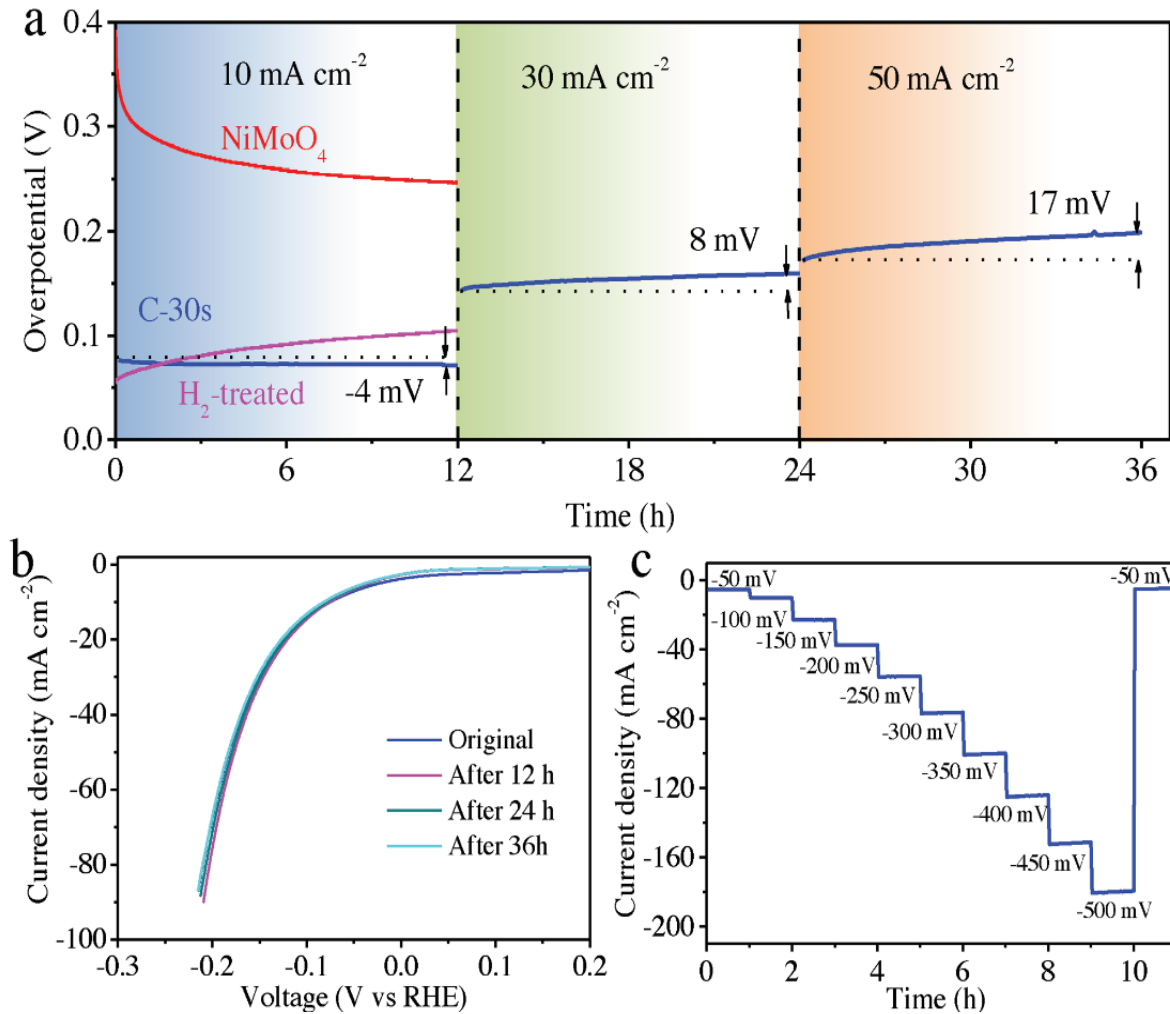
- **XRD patterns confirm** that NiMoO₄ was **converted into Ni₄Mo** and MoO₂ after 30 s C-plasma treatment.

Example 3: Prereduction of MO by Carbon Plasma for Efficient and Stable HER



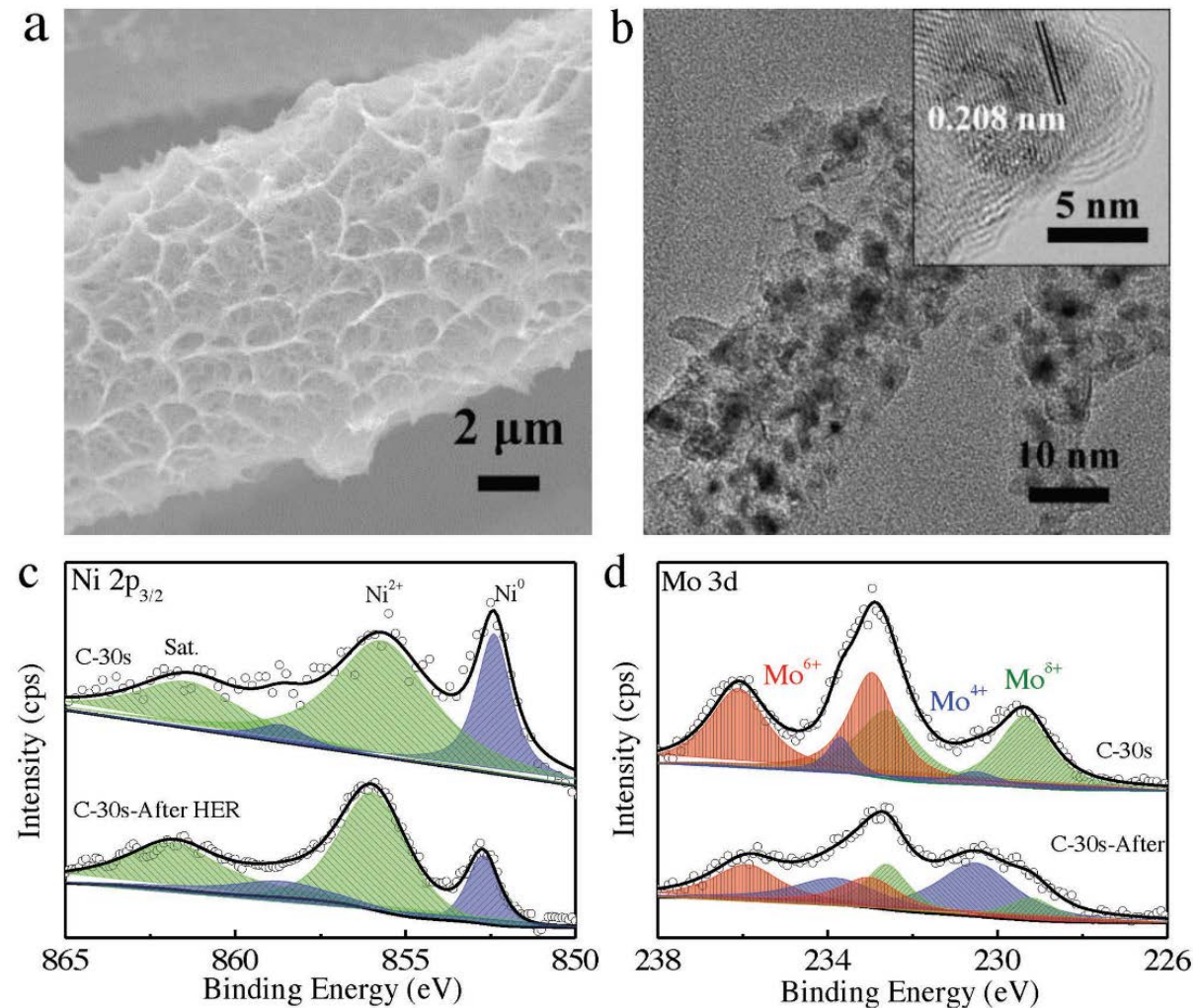
- Order of HER activity increase: NiMoO₄ \rightarrow C-15s \rightarrow C-60s \rightarrow C-30s \rightarrow Pt/C
- Overpotential of only 76 mV is required for C-30s to reach a current density of 10 mA cm^{-2} (η_{10}), which is slightly higher than that of Pt/C (45 mV) but lower than that of NiMoO₄ (406 mV), C-15s (135 mV), and C-60s (152 mV).
- Inferior HER activity of C-60s \rightarrow thicker & hollow C shell \rightarrow active sites blocking
- The Tafel slope (Fig b) of C-30s (78 mV dec^{-1}) is smaller than those of NiMoO₄ (130 mV dec^{-1}), C-15s (106 mV dec^{-1}), and C-60s (103 mV dec^{-1}) – Note: Smaller Tafel slope \Rightarrow better HER reaction kinetics
- The comparison of Tafel slope versus η_{10} value (Fig c) \rightarrow the C-plasma treated NiMoO₄ significantly better HER catalytic activity (larger current density and faster HER rates).
- The typical Nyquist plots from EIS in Figure 3d depict the diameter smallest semicircle for C-30s, indicating that it has the fastest electron transfer and HER activation.

Example 3: Prereduction of MO by Carbon Plasma for Efficient and Stable HER



- The C-30s sample also exhibits an excellent long-term electrochemical stability.
- Overpotential for electrolysis at three constant current densities (10, 30, and 50 mA cm⁻²) shows a relatively small fluctuation after each 12 h electrolysis (-4, 8, and 17 mV at 10, 30, and 50 mA cm⁻², respectively).
- The slight decrease of overpotential at 10 mA cm⁻² was probably due to the penetration of electrolyte to expose more active sites.
- The degradation at 30 and 50 mA cm⁻² was partially due to reduced active sites caused by the physical adsorption of the generated H₂.
- Figure 4b - the linear sweep voltammetry (LSV) curves after electrolysis at different current densities almost overlap with the original one.

Example 3: Prereduction of MO by Carbon Plasma for Efficient and Stable HER



- The nanowire array morphology and the layer of carbon shell were well preserved, as shown by SEM and TEM images in Fig a,b.
- The Ni₄Mo nanoparticles are clearly observed in nanowires, owing to the protection provided by the carbon shell.
- The XPS peaks due to both Ni⁰ and Mo^{δ+} remain except for slight decrease in their intensities.
- This verifies that the C-30s sample is not only a highly active but also a very stable electrocatalyst for HER in alkaline medium.

Outline of Presentation

Introduction – Energy Conversion and Plasmas,

- Hydrogen Economy (Energy Conversion)
- Our focus - plasma based strategies
- Plasma processing/depositions for EC-Energy conversion/storage Materials

Some examples of application of low temperature nitrogen plasmas for energy Conversion applications

Recent work - Facet Control of Ni₃N Nano-Framework for Efficient HER via Auxiliary Cooling Assisted Plasma Engineering

Conclusions

Example 4: Facet Control of Ni₃N Nano-Framework for Efficient HER via Auxiliary Cooling Assisted Plasma Engineering

- Liu et al reported Ni₃N and WN fabrication by plasma technique with reasonably good HER performance^[a,b] - demonstrating superiority of plasma technique.
- However, the achieved nitrides using plasma techniques usually delivered the structural features, similar to that obtained by thermal nitridation. For instance, **both thermally- and plasma-fabricated Ni₃N deliver the hexagonal structure with exposed facet of (2-11)** on the surface and such facet provides unsatisfied catalytic activity based on theoretical simulation.^[c]
- **Exposing more reactive facets is regarded as the essential factor** to significantly enhance catalytic activity. Hence, exploring an efficient strategy to achieve TMNs with expected facets is highly desirable for electrocatalysis.
- We reported a novel **cold plasma strategy^[d] to modulate exposed facets of Ni₃N through controlling surface heating effect during plasma processing.** The resultant nano-framework yields desired (2-10) facet on coralline surface which provides better HER performance.

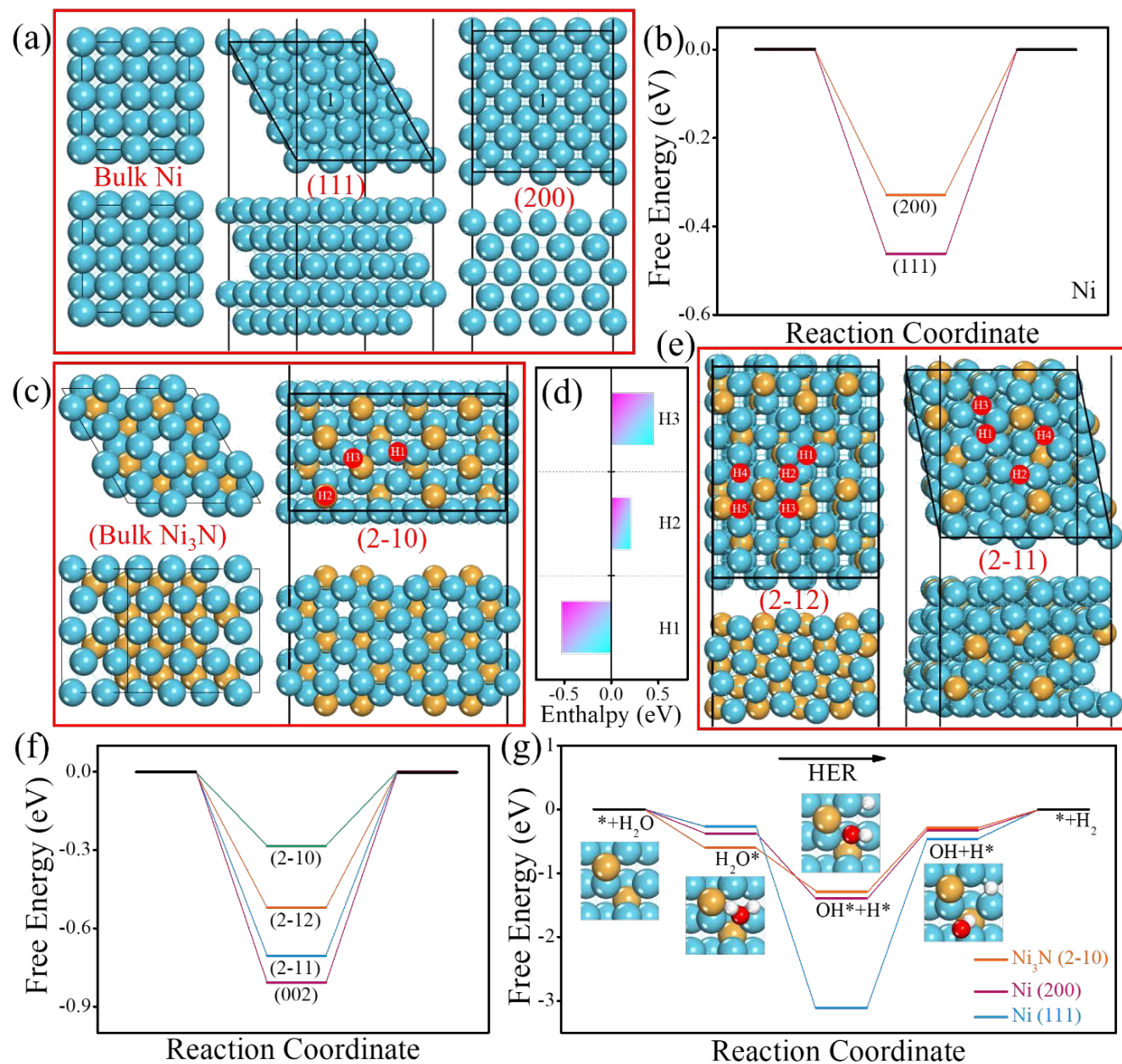
a. B. Liu, B. He, H.-Q. Peng, Y. Zhao, J. Cheng, J. Xia, J. Shen, T.-W. Ng, X. Meng, C.-S. Lee, W. Zhang, *Adv. Sci.* **2018**, *5*, 1800406.

b. B. Liu, D. Li, Q. Jin, H. Cui, C. Wang, *J. Mater. Chem. A* **2017**, *5*, 19072-19078.

c. S. Hu, S. Wang, C. Feng, H. Wu, J. Zhang, H. Mei, *ACS Sustain. Chem. Eng.* **2020**, *8*, 7414-7422.

d. Ouyang, B., Zhang, Y., Wang, X., Deng, Y., Liu, F., Fang, Z., **Rawat, R. S.***, & Kan, E.* (2022) Facet Control of Nickel Nitride Nano-Framework for Efficient Hydrogen Evolution Electrocatalysis via Auxiliary Cooling Assisted Plasma Engineering, *Small*, *18*(49) 2204634.

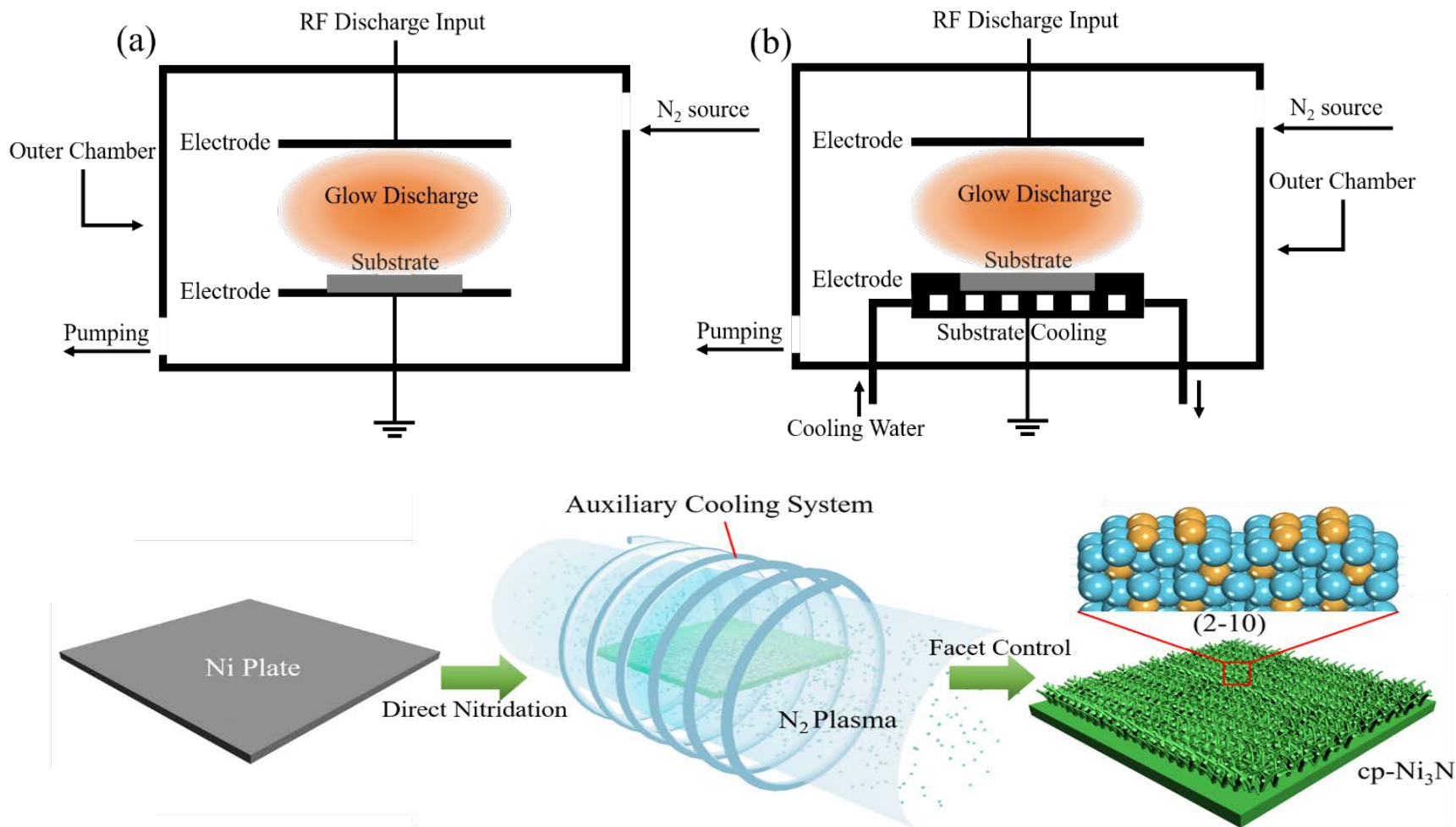
Example 4: Facet Control of Ni₃N Nano-Framework for Efficient HER via Auxiliary Cooling Assisted Plasma Engineering



DFT predicted HER free energy diagrams of Ni and Ni₃N structure models in alkaline condition. (a) top and side view of bulk Ni along with its (111) and (200) facets, (b) free energy for HER on typical facets of cubic Ni model, (c) top and side view of bulk Ni₃N along with its (2-10) facet, (d) the H-absorbing energy on active sites of Ni₃N (2-10), (e) top and side view of Ni₃N (2-12) and (2-11) facets, (f) free energy for HER on typical facets of hexagonal Ni₃N model, (g) comparison of free energy diagram for HER on typical facets of Ni and Ni₃N in **alkaline condition**.

- For Ni - reduced energy barrier, -0.33 eV, of H-desorption for (200) facet → better catalytic behavior than (111) facet which has -0.47 eV barrier (see Fig. b)
- For Ni₃N – H1-site Ni-H-Ni bond is most favorable for H-absorption (-0.5 eV) compared to H2-site Ni-H (+0.2 eV) & H3-site Ni-N-H (+0.5 eV) bonds (see Fig. d)
- In terms of ΔG_{H^*} (Gibbs free energy for H-adsorption - the (2-10) facet exhibits much improved HER activity with ΔG_{H^*} of -0.28 eV, superior to those of other facets of Ni₃N (Fig. f) and Ni (Fig. b) and even that of Pt (-0.29 eV) → **suggesting that Ni₃N with (2-10) facet is a theoretically promising substrate during HER process in alkaline condition**

Example 4: Facet Control of Ni₃N Nano-Framework for Efficient HER via Auxiliary Cooling Assisted Plasma Engineering

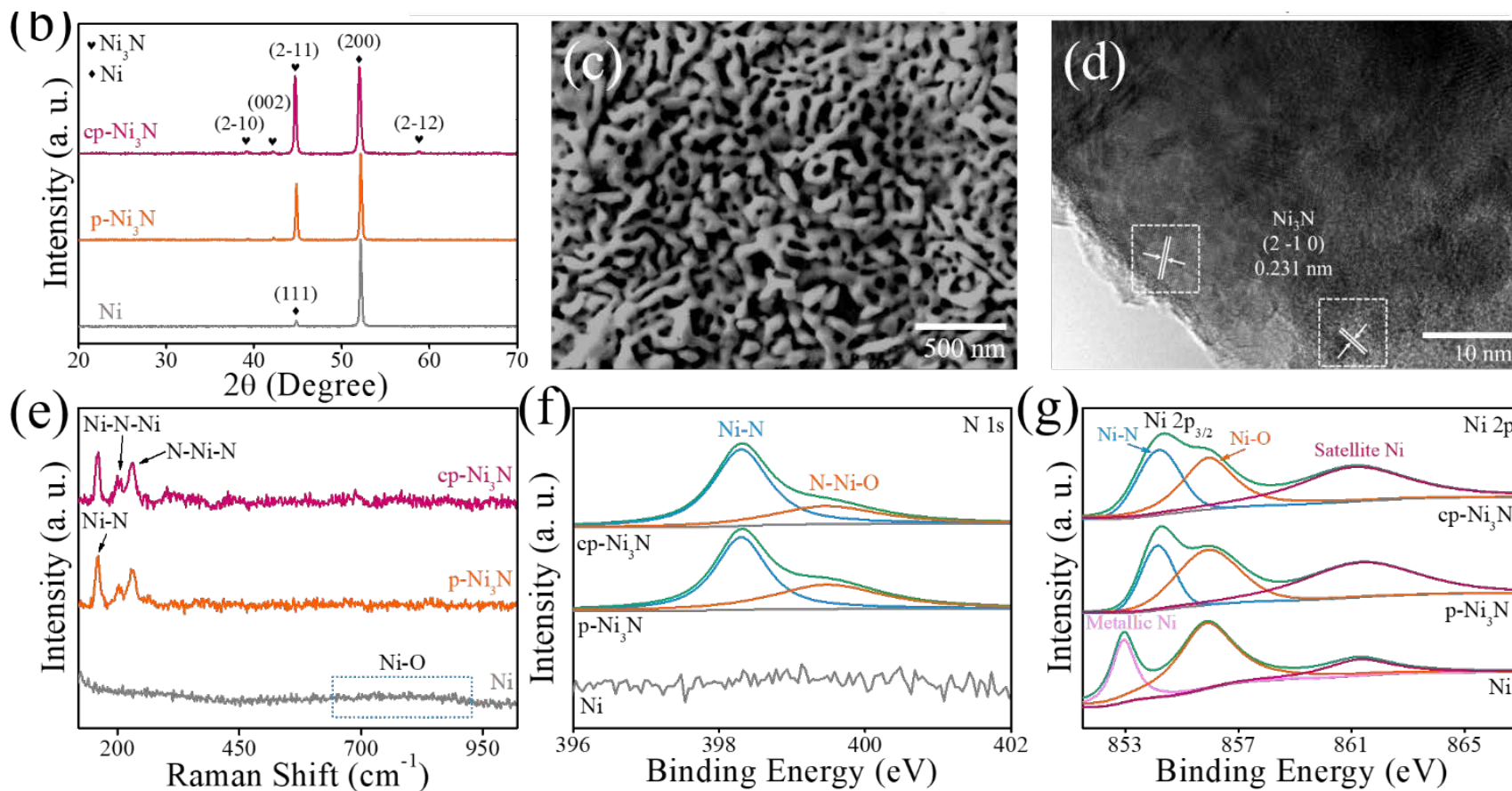


p-Ni₃N Preparation: Ni plate was cleaned ultrasonically with acetone and 3 M HCl solution several times. N₂ gas was flown at 40 sccm with chamber pressure kept at ~30 Pa. Nitrogen plasma by Caeser136 RF generator (500 W, 13.56 MHz) for 300 s of nitridation.

cp-Ni₃N Preparation: Same as above but with Ni substrate surface temperature during plasma nitridation controlled by adjusting cooling water flow rate.

Thermal Nitridation (T-Ni₃N): Same as other reported work – using highly purified NH₃ at a flow rate of 40 sccm to quartz chamber with Ni substrate. After stabilizing gas flow, the furnace temperature was increased to different temperature with raising rate of 5 °C min⁻¹ for 2 h. The obtained hNi₃N with different processing temperature of 400, 500 and 600 °C, was named as T-Ni₃N-X (X=400, 500, 600).

Example 4: Facet Control of Ni₃N Nano-Framework for Efficient HER via Auxiliary Cooling Assisted Plasma Engineering

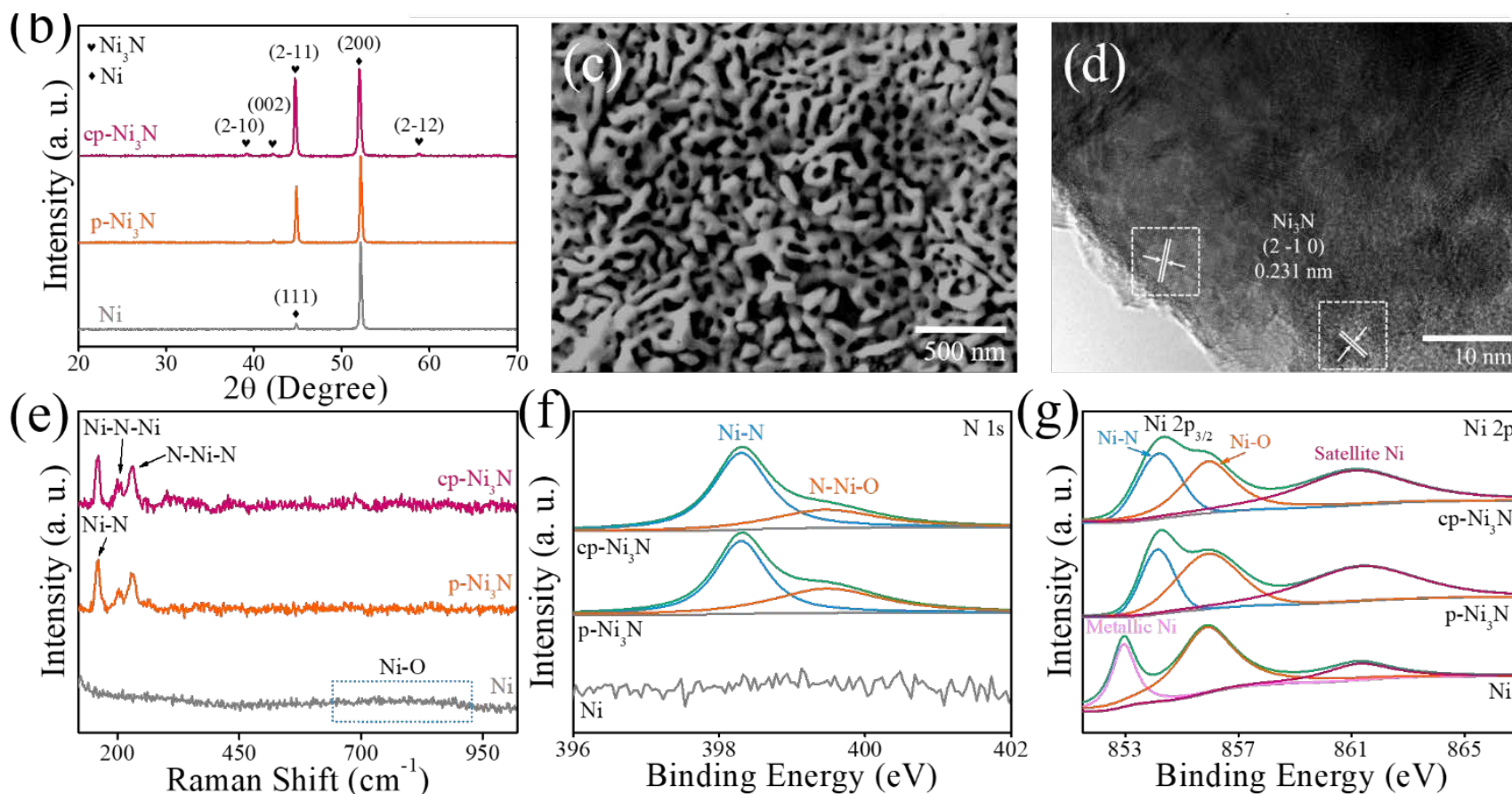


XRD Results: Both p-Ni₃N and cp-Ni₃N have peaks at 39.3°, 42.1°, 44.6° and 58.7°, corresponding to (2-10), (002), (2-11) and (2-12) of hexagonal Ni₃N. Ni substrate only shows characteristic peaks of (111) and (200) peaks. The intensity of Ni₃N (2-10) in cp-Ni₃N is two times that in p-Ni₃N, indicating increased (2-10) formation on cp-Ni₃N.

SEM Results; cp-Ni₃N exhibits a nano-coral structure (Fig. c) with a mean diameter of 45 nm, which is larger than the 22 nm mean diameter of nano-corals of p-Ni₃N, which has increased roughness. Surface heating effects in p-Ni₃N cause roughening of the nano-coral structure. The cooling process in cp-Ni₃N limits the penetration of reactive N-species and the kinetics of nickel ions, and hence reduces roughness.

Characterizations of Ni, p-Ni₃N and cp-Ni₃N: (b) XRD patterns, (c) and (d) SEM and TEM images of cp-Ni₃N, (e) Raman spectra, (f) XPS N 1s spectra, (g) XPS Ni 2p spectra.

Example 4: Facet Control of Ni₃N Nano-Framework for Efficient HER via Auxiliary Cooling Assisted Plasma Engineering



TEM Results: of cp-Ni₃N (Fig. d) the exposed facets are mainly (2-10) facet, in comparison with (2-11) of p-Ni₃N (not shown), indicating different facet exposure due to auxiliary cooling.

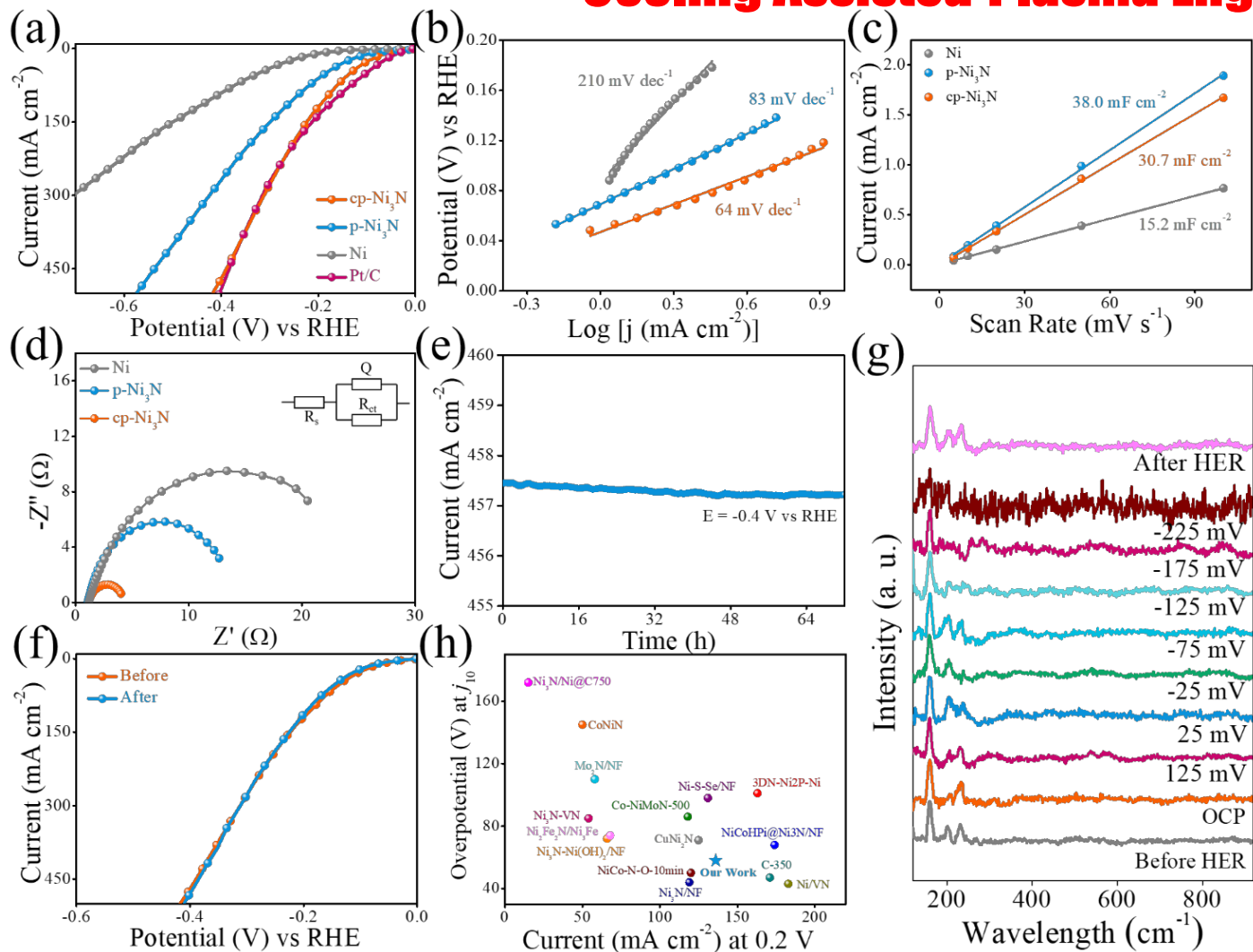
Raman Spectra: of both samples have peaks at 160, 199 & 228 cm⁻¹ of Ni-N, Ni-N-Ni and N-Ni-N vibrations, respectively, confirming Ni₃N formation.

XPS N 1s: both p- & cp-Ni₃N have peak at 398.3 eV, indicating the Ni-N bonding (NiN_x formation). The peak at 399.5 eV, indicates N-Ni-O (NiO_x formation). The intensity ratio of NiN_x/NiO_x for cp-Ni₃N is 2.37, which is higher than 1.51 for p-Ni₃N - showing more effective plasma nitridation for cooled substrate.

Characterizations of Ni, p-Ni₃N and cp-Ni₃N: (b) XRD patterns, (c) and (d) SEM and TEM images of cp-Ni₃N, (e) Raman spectra, (f) XPS N 1s spectra, (g) XPS Ni 2p spectra.

XPS Ni 2p: both p- & cp-Ni₃N have peak at 854.0 eV corresponding to Ni-N bonding. Ni has two peaks at 853.1 and 856.0 eV corresponding to metallic Ni and Ni-O. Ni-O bonding peak is also found on both p-Ni₃N and cp-Ni₃N surfaces → O₂-absorption on nitride surface due to contact of Ni₃N with air. Higher proportion of O-related peak in p-Ni₃N than that in cp-Ni₃N, again confirms the advantages of using cooled substrate.

Example 4: Facet Control of Ni₃N Nano-Framework for Efficient HER via Auxiliary Cooling Assisted Plasma Engineering

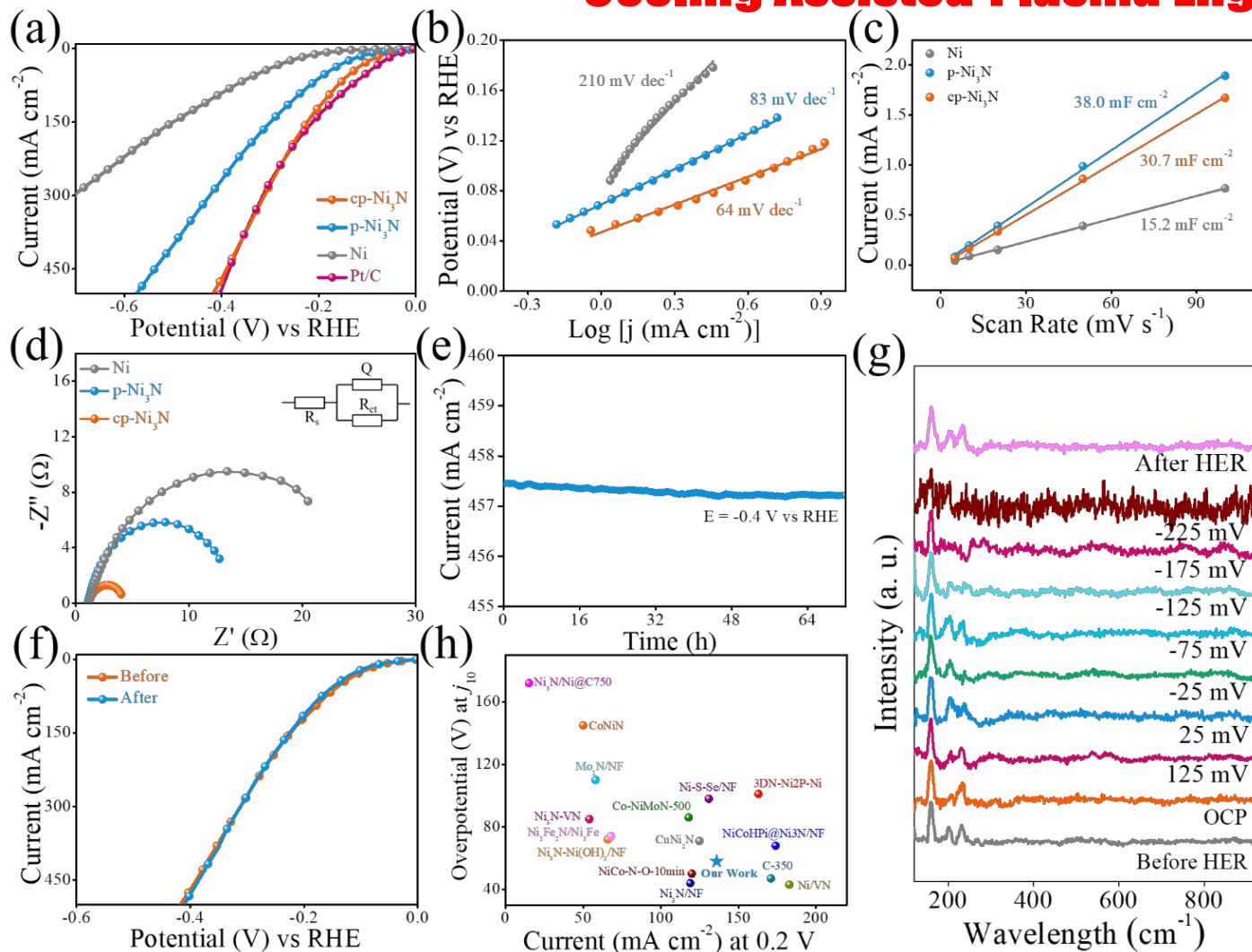


- IR-corrected linear sweep voltammetry (LSV) curves (Fig a): cp-Ni₃N presents much enhanced electrocatalytic activity with overpotential of 58 mV at current density of 10 mA cm⁻² (j_{10}), much lower than that of p-Ni₃N (93 mV) and pure Ni (203 mV). Pt/C electrode commonly achieves the lowest j_{10} of 38 mV, and our cp-Ni₃N is almost comparable with noble metal-based catalyst.

- Tafel slopes of cp-Ni₃N is 64 mV dec⁻¹, smaller than that of p-Ni₃N (83 mV dec⁻¹) and Ni (210 mV dec⁻¹) - further confirms the difference of exposed facet. Tafel slope value in the range of 40-120 mV dec⁻¹ implies HER in cp-Ni₃N proceeds through a Volmer-Heyrovsky mechanism during which the electrochemical hydrogen desorption serves as the essential step. Our cp-Ni₃N electrode exhibits comparable and even superior Tafel slope as compared to CoNi₂N (80.1 mV dec⁻¹), NiCo-N-O-10 (112 mV dec⁻¹), CuNi₂N (106.5 mV dec⁻¹), and VN (96 mV dec⁻¹) demonstrating advantage of exposed (2-10) facet in cp-Ni₃N.

Electrocatalytic HER behaviors of p- & cp-Ni₃N. (a) LSV curves with scan rate of 10 mV s⁻¹, (b) Tafel plots, (c) Plots for extraction of double-layer capacitance (C_{dl}), (d) Nyquist plots, (e) chrono-potentiometric curve of cp-Ni₃N, (f) LSV curves before and after stability test, (g) operando Raman spectra during HER process, (h) comparison between cp-Ni₃N and typical electrocatalysts in overpotential and current density.

Example 4: Facet Control of Ni₃N Nano-Framework for Efficient HER via Auxiliary Cooling Assisted Plasma Engineering



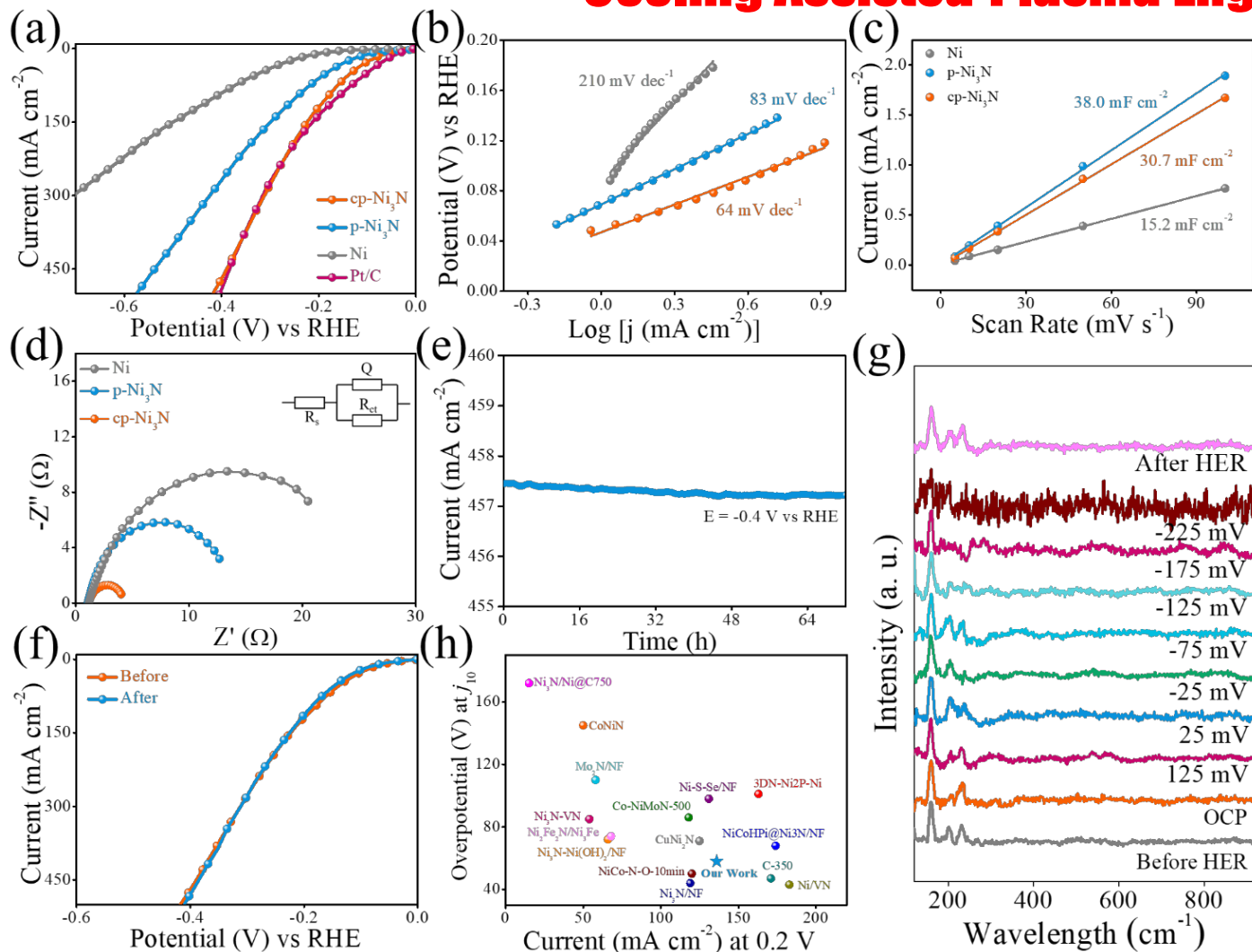
- The measurement of electrochemically active surface area (ECSA) through estimated double-layer capacitance C_{dl} is important to understand HER performance. Among all samples, the C_{dl} of p-Ni₃N is 38.0 mF cm⁻², higher than that of cp-Ni₃N (30.7 mF cm⁻²) and Ni (15.2 mF cm⁻²), refer **Fig. c**, indicating reduced surface area for cp-Ni₃N (consistent to SEM results). **However, cp-Ni₃N delivers enhanced catalytic behavior with even lower ECSA compared to p-Ni₃N**, suggesting that exposed (2-10) facet provides a critical role in promoting HER process rather than the function of active area.

- The Nyquist plots in **Fig. d**, shows that cp-Ni₃N catalyst exhibits a charge transfer resistance (R_{ct}) of 3.2 Ω , significantly smaller than that of p-Ni₃N (13.5 Ω) and Ni (26.7 Ω), which further indicates the improved charge transfer behavior of cp-Ni₃N.

- Fig. e** shows little current decay for 72 h with constant potential of -0.4 V (vs RHE) \rightarrow stable performance

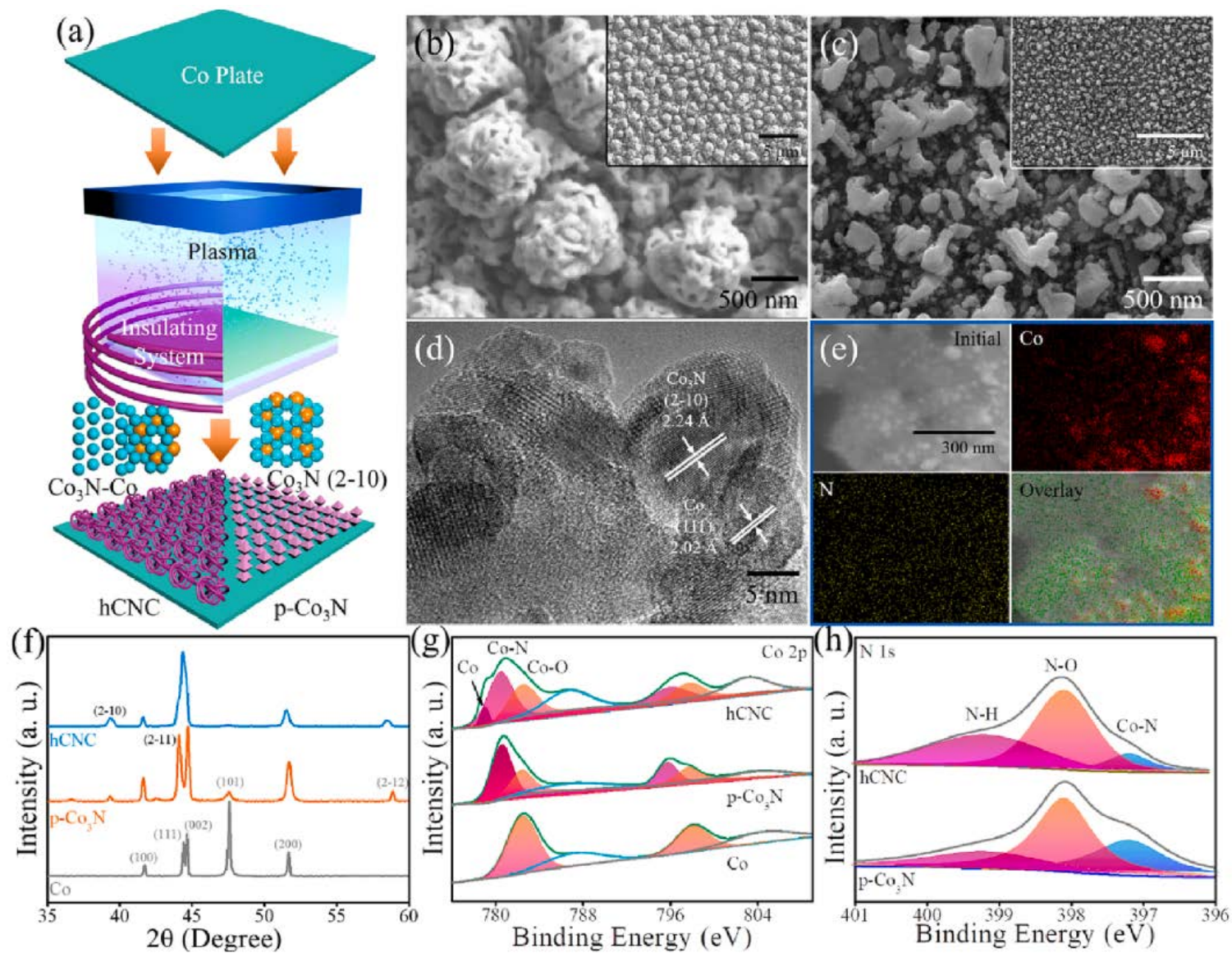
Electrocatalytic HER behaviors of p- & cp-Ni₃N. (a) LSV curves with scan rate of 10 mV s⁻¹, (b) Tafel plots, (c) Plots for extraction of double-layer capacitance (C_{dl}), (d) Nyquist plots, (e) chrono-potentiometric curve of cp-Ni₃N, (f) LSV curves before and after stability test, (g) operando Raman spectra during HER process, (h) comparison between cp-Ni₃N and typical electrocatalysts in overpotential and current density.

Example 4: Facet Control of Ni₃N Nano-Framework for Efficient HER via Auxiliary Cooling Assisted Plasma Engineering



- Fig. f** shows the LSV plots before and after stability test. There is negligible potential increment. Tafel slope values before and after cycling (Fig. S15) for cp-Ni₃N electrode increased from 64 to 78 mV dec⁻¹, which is ascribed to the partial degradation of catalyst.
- Fig. g** shows the operando-Raman spectra of cp-Ni₃N during HER process. Ni₃N-related peaks are observed during catalytic process without any shift, indicating the excellent structural stability of cp-Ni₃N. Notably, only at overpotential of -225 mV peak seems to disappear, which is ascribed to the generation of large amounts of H₂ bubbles at high potential and hence interference of signals. The Ni₃N peak reemerges after HER process, indicating its great structural stability.
- Our cp-Ni₃N electrode delivers comparable and even superior overpotential along with current density in comparison with most other reported catalysts (**Fig. h**).

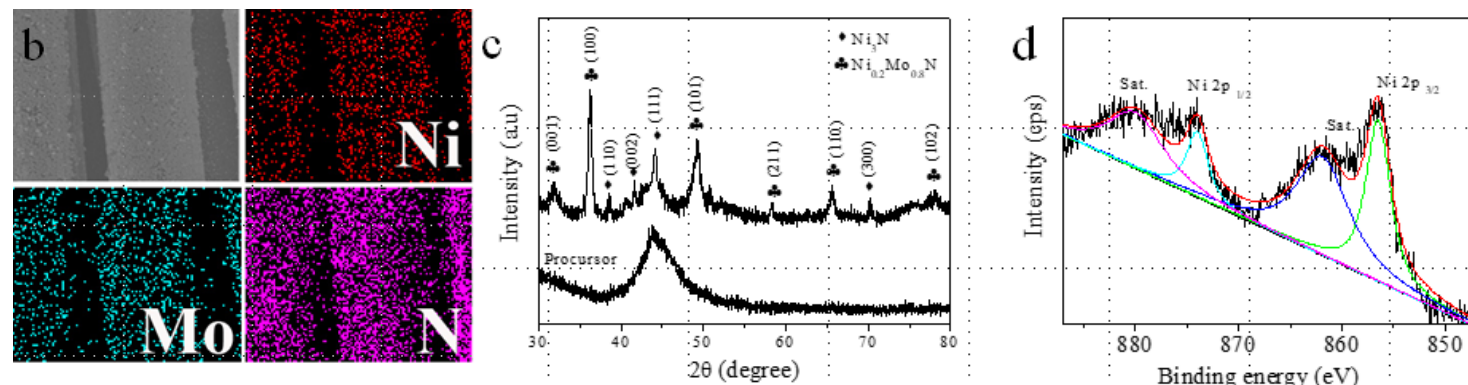
Example 5: Heterostructured Co₃N-Co nano-corals for enhanced electrocatalytic HER based on insulator-confined plasma engineering



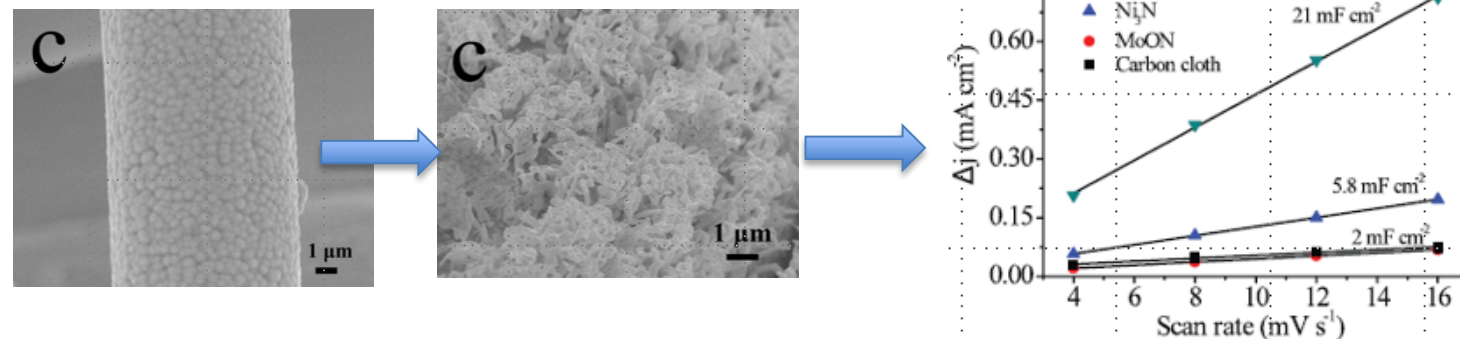
- To achieve HER behavior, we design auxiliary insulator-confined plasma system to directly achieve Co₃N-Co heterostructure (hCNC) with favorable activity by controlling surface heating process during plasma nitridation.
- The resultant hCNC nano-framework delivers excellent catalytic performance, evidenced by its overpotential of 97 and 229 mV at current density of 10 and 100 mA cm⁻² for HER in alkaline condition, in stark comparison with that of normal plasma fabricated Co₃N.
- Operando plasma diagnostics along with numerical simulation confirmed the effect of surface heating on typical plasma parameters as well as the Co₃N-Co nano-structure, indicating the key factor responsible for the high-performance hetero-structured electrocatalyst.

Conclusion: Plasma can tune surface properties of electrocatalyst for enhanced EC performance by

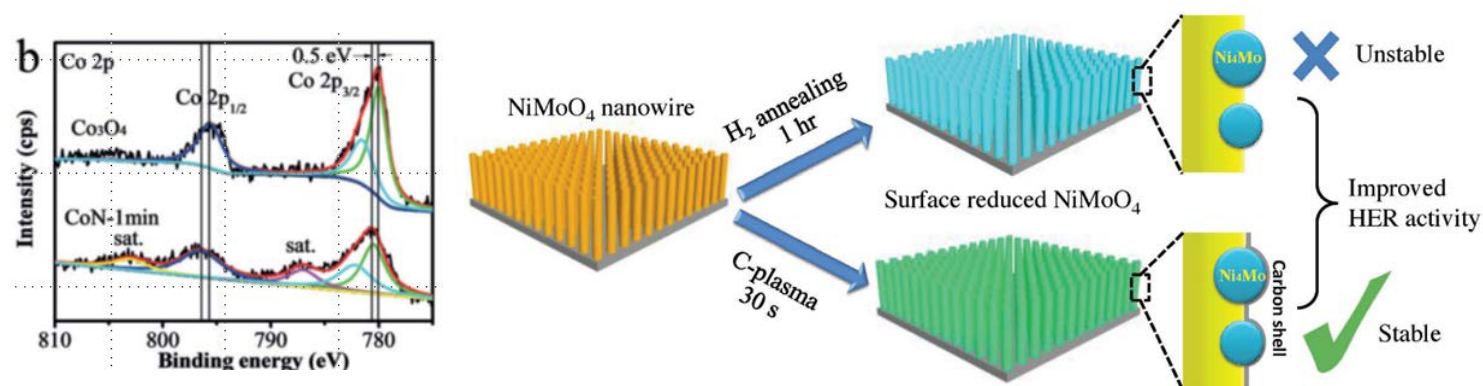
1) **Surface functionalization** by excited radical species - resulting in new doping functionalities.



2) **Surface re-texturing** to increase roughness and porosity.

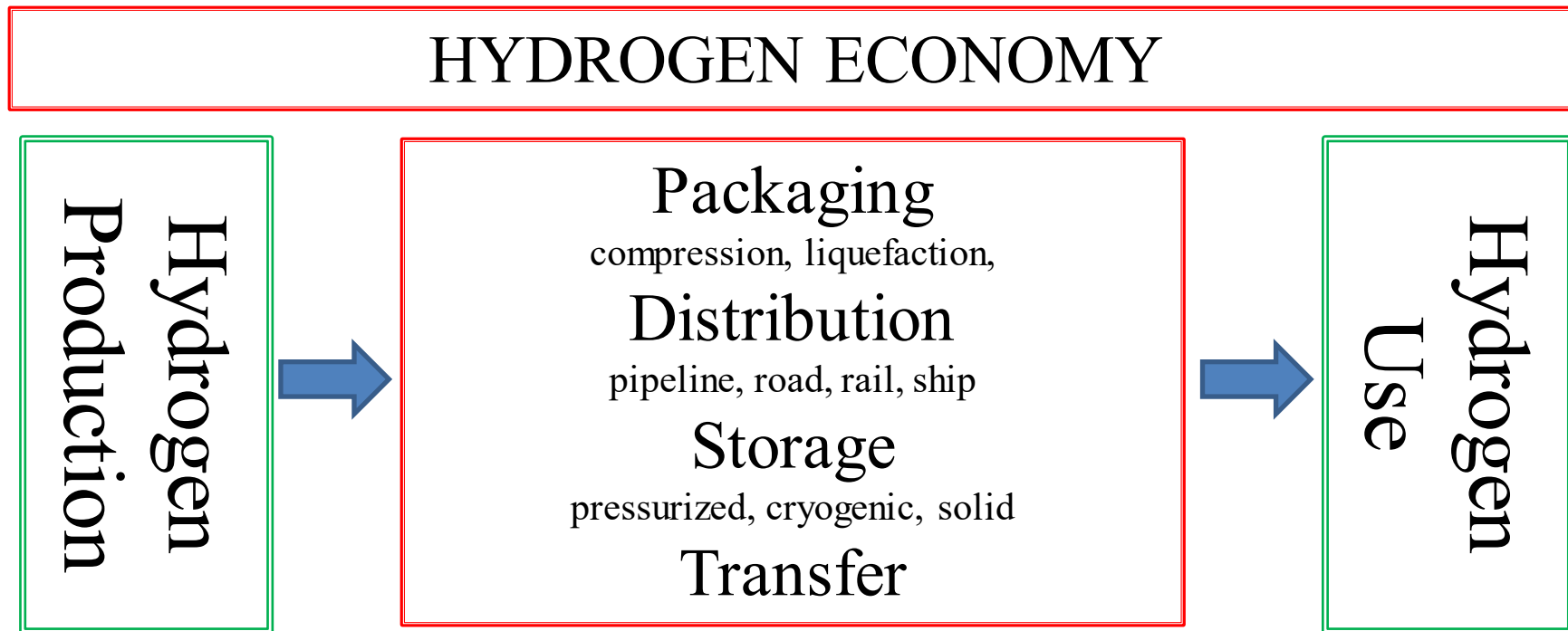


3) **By partially reducing** or oxidizing the material surface to tune the electronic properties of the active sites.

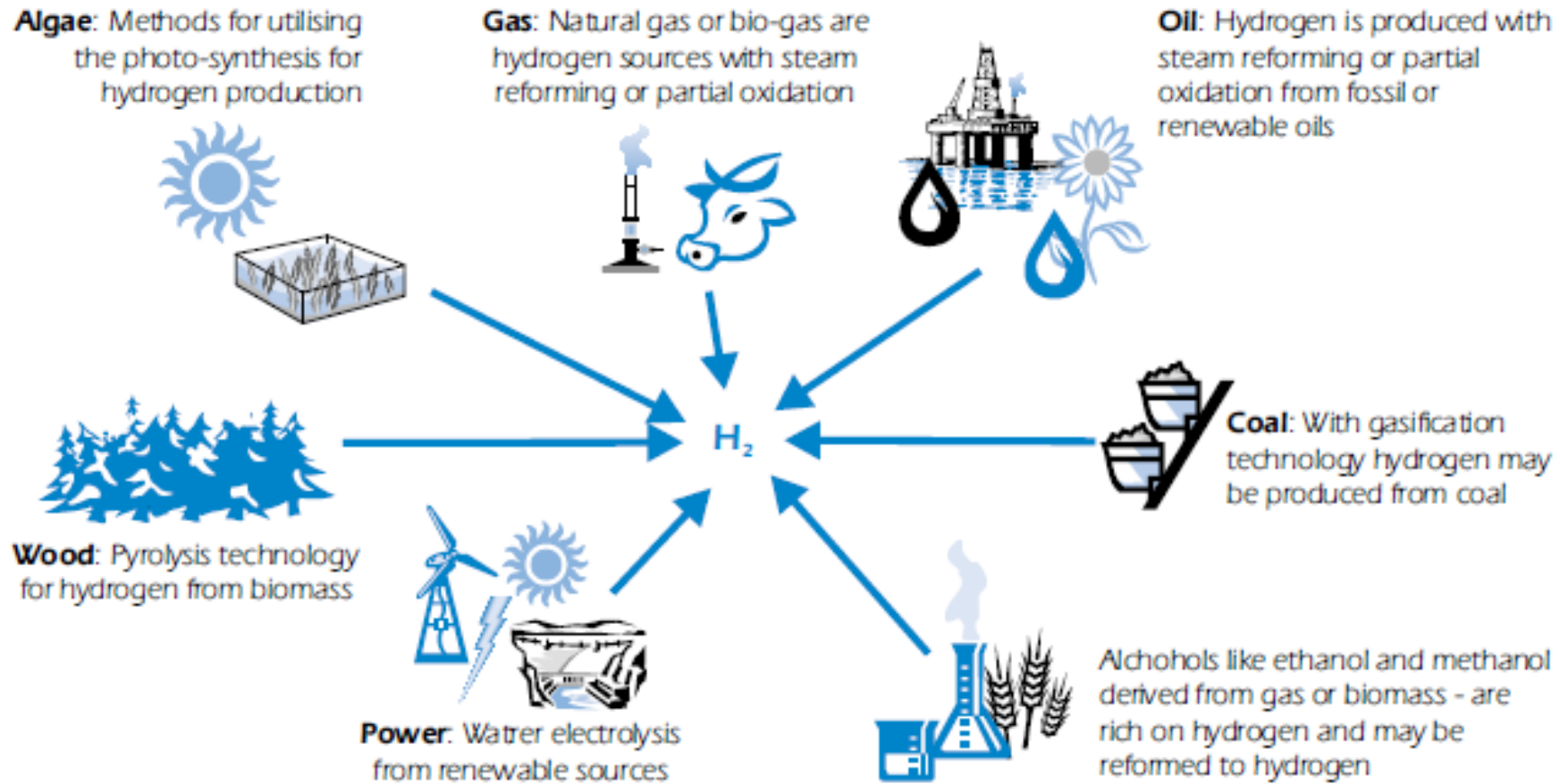


Energy Conversion - Hydrogen Economy

- Hydrogen is likely to be an important part of carbon-neutral/carbon future
- A hydrogen molecule (H_2) in the presence of oxygen can be converted to water with a release of heat and work.
- The “hydrogen economy” is a system that uses hydrogen as a major carrier in the energy supply cycle.



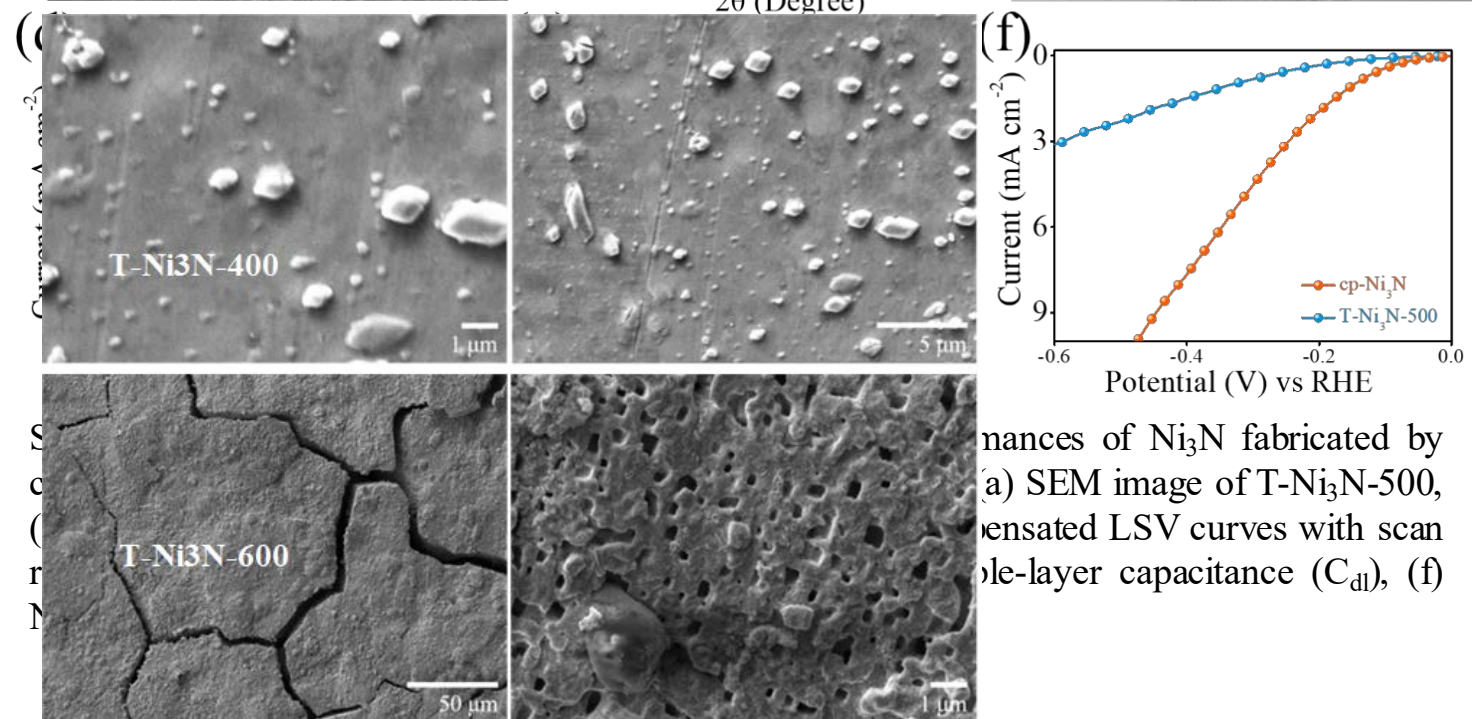
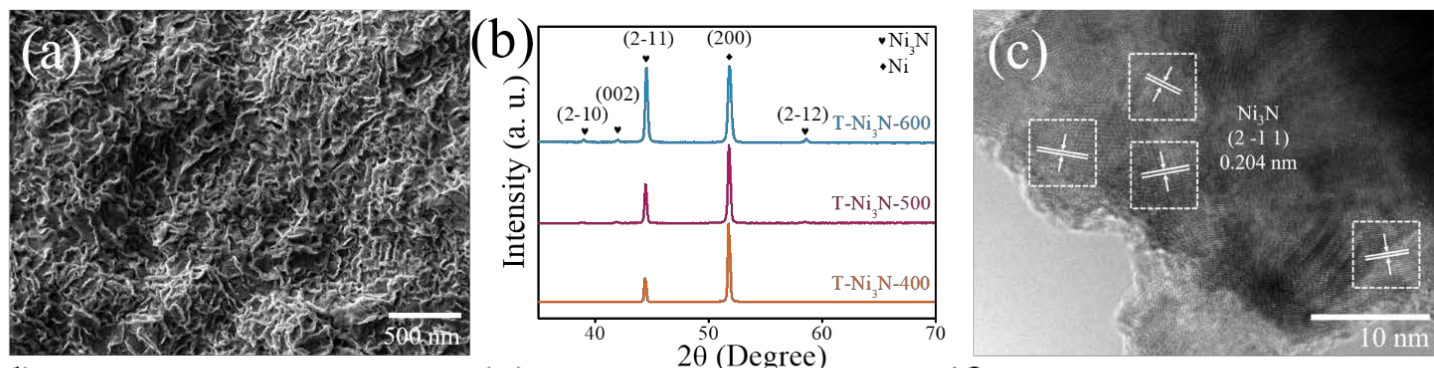
Hydrogen Production : Many Alternatives



Source: Hydro.

There are seven key production methods which can be broadly classified into three main process.

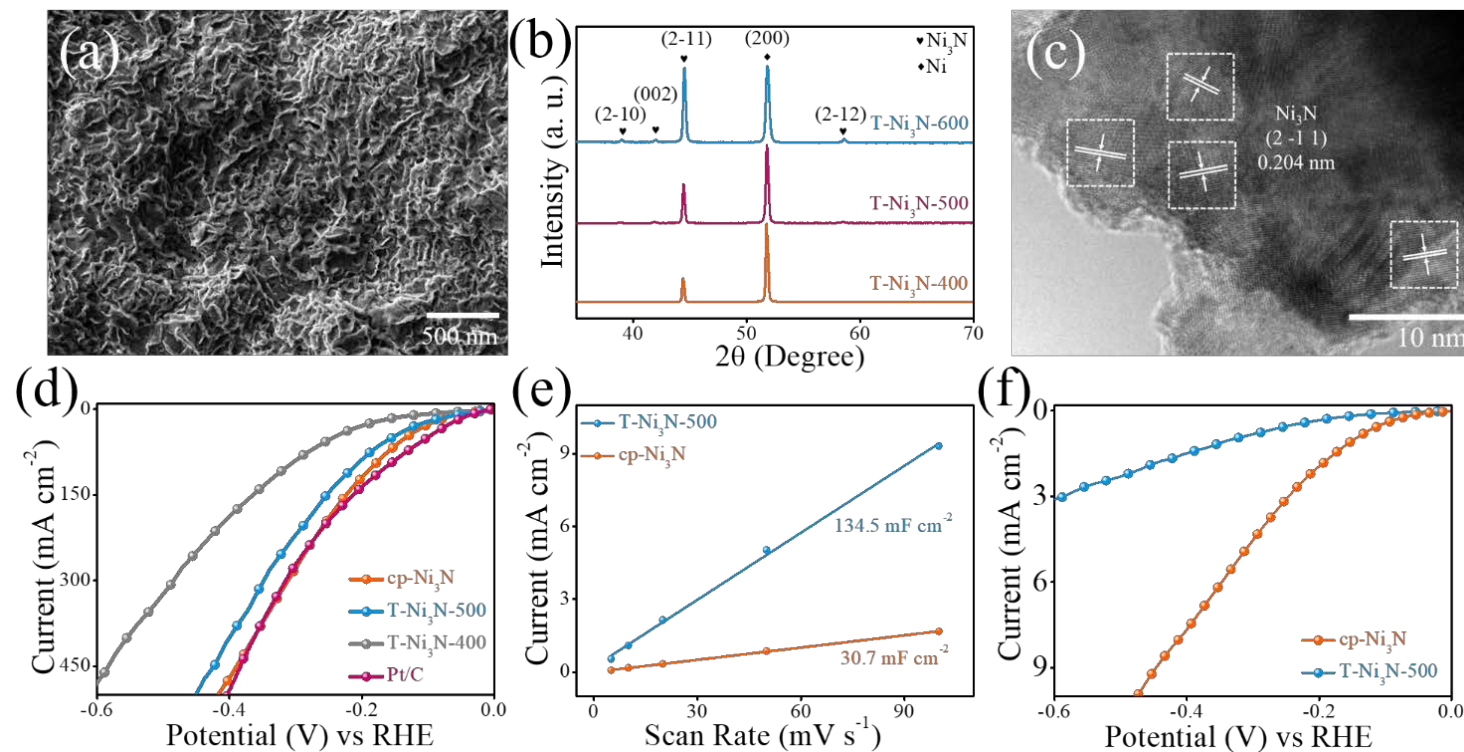
Example 3: Facet Control of Ni₃N Nano-Framework for Efficient HER via Auxiliary Cooling Assisted Plasma Engineering



performances of Ni₃N fabricated by (a) SEM image of T-Ni₃N-500, (b) LSV curves with scan rate of 10 mV s⁻¹, (c) double-layer capacitance (C_{dl}), (f)

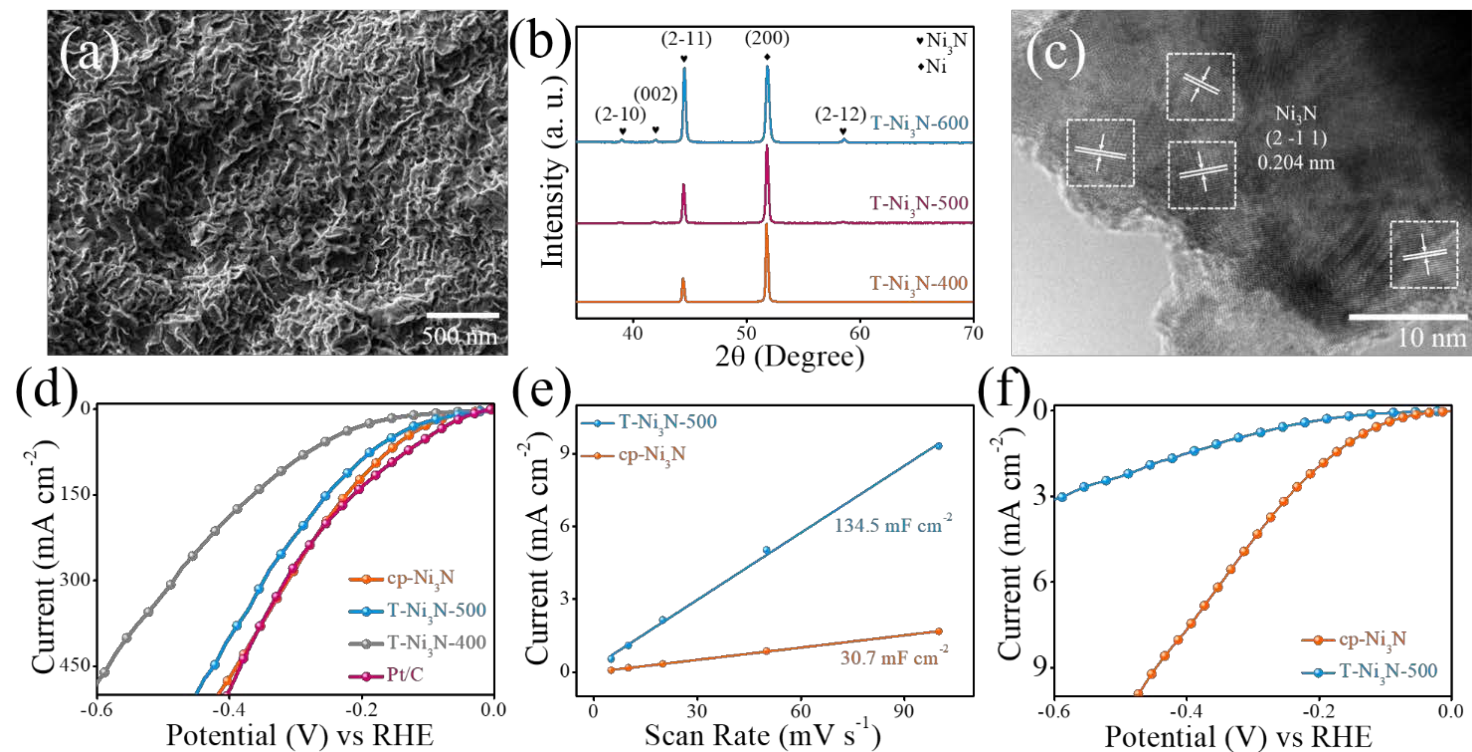
- The T-Ni₃N fabricated by conventional thermal nitridation is further applied for comparison.
- SEM images show that the surface morphology of prepared T-Ni₃N is apparently different based on NH₃ annealing from 400 to 600 °C.
- For T-Ni₃N-400 (thermally nitrided Ni₃N at 400 °C), there are separately distributed nanoparticles on Ni surface, inducing little nitride formation at such low temperature.
- With raised nitriding temperature at 500 °C (Fig a), highly **roughened frameworks** are generated on Ni surface, suggesting nickel nitride formation.
- The T-Ni₃N-600 shows the nanopore expansion, nitride aggregation and even partial pulverization of Ni₃N, which can hardly be used as the free-standing electrode.

Example 3: Facet Control of Ni₃N Nano-Framework for Efficient HER via Auxiliary Cooling Assisted Plasma Engineering



- XRD Results (Fig. b):** The well-defined peaks corresponding to Ni₃N are observed with thermal nitridation at 600 °C. No peaks ascribed to (2-10), (002) and (2-12) can be found with nitridation at 400 °C.
- TEM Results (Fig. c):** of T-Ni₃N-500 mainly shows (2-11) facet on its surface, same with that of p-Ni₃N, confirming that surface heating process promotes the generation of (2-11) facet and simultaneously hinders the exposure of (2-10) facet in nickel nitride.
- Fig d -** the overpotential of T-Ni₃N-500 is 58 mV at j_{10} , similar with that of cp-Ni₃N. With increased current densities, it delivers overpotential of 154 and 209 mV at j_{50} and j_{100} , higher than that of cp-Ni₃N. Comparatively, T-Ni₃N-400 provides much inferior overpotential owing to little formation of metal nitride.

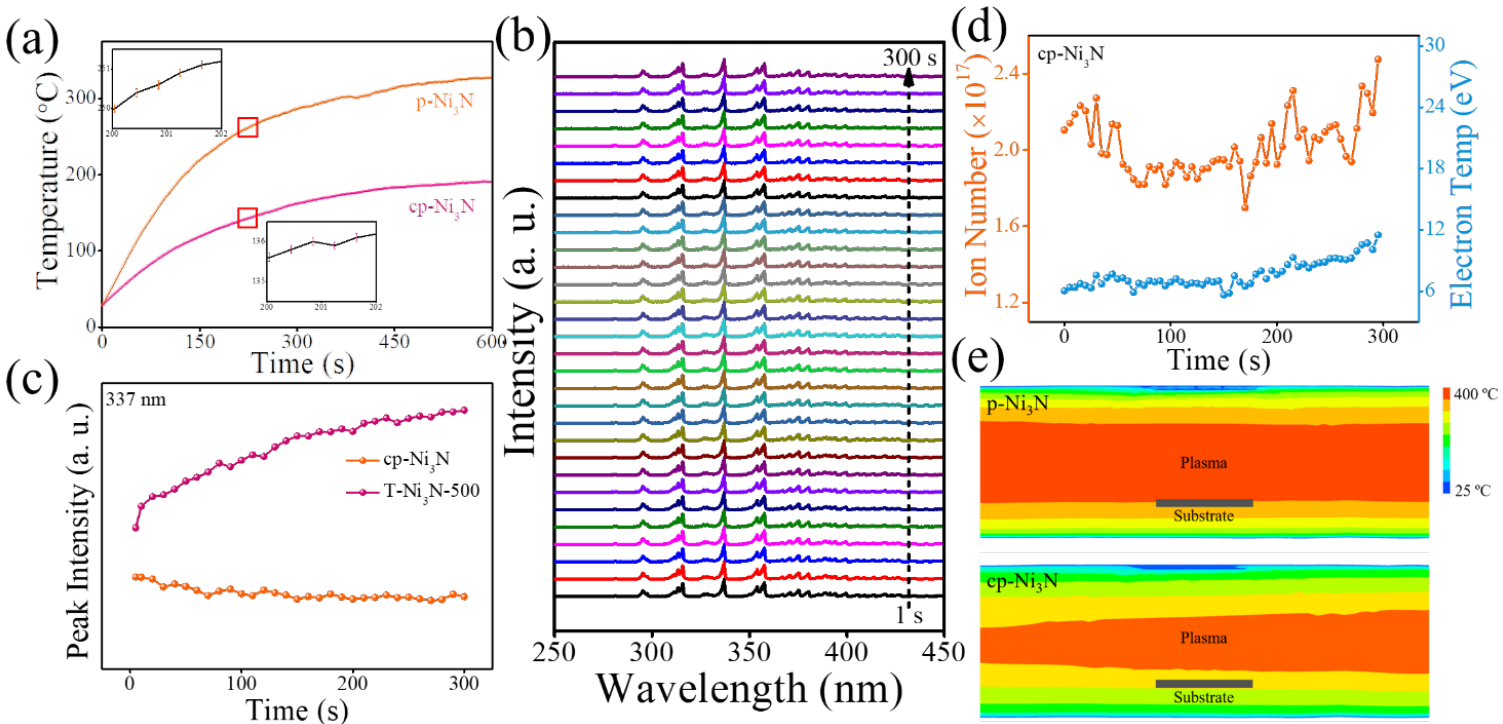
Example 3: Facet Control of Ni₃N Nano-Framework for Efficient HER via Auxiliary Cooling Assisted Plasma Engineering



- ECSA Results (Fig. e):** shows that T-Ni₃N-500 provides much larger surface area than that of cp-Ni₃N, which is attributed to the accelerated kinetics of Ni ions reacting with NH₃ at high temperature. However, such enhanced ECSA did lead to the improved HER behavior, indicating the importance of exposed facets in affecting electrocatalytic process.
- Based on normalized LSV curves by ECSA (Fig. f), the cp-Ni₃N exhibits much enhanced current density at the same overpotential compared to T-Ni₃N-500, further confirming that the improved catalytic activity is derived from (2-10) facet.

Structural Characterizations and Electrocatalytic HER performances of Ni₃N fabricated by cooling plasma and thermal nitridations in alkaline condition. (a) SEM image of T-Ni₃N-500, (b) XRD patterns, (c) TEM image of T-Ni₃N-500, (d) iR-compensated LSV curves with scan rate of 10 mV s⁻¹, (e) The plot from the extraction of double-layer capacitance (C_{dl}), (f) Normalized LSV curves by ECSA.

Example 3: Facet Control of Ni₃N Nano-Framework for Efficient HER via Auxiliary Cooling Assisted Plasma Engineering



Operando plasma diagnostics and finite element analysis of plasma and cooling plasma nitridation. (a) in-situ infrared temperature measurement, (b) time-dependent OES spectra, (c) the variation of peak intensity with processing duration, (d) the variation of ion density and electron temperature with processing duration, (e) finite element simulation.

- Fig. a:** in-situ infrared thermography show that substrate surface temperature during plasma processing with and without auxiliary cooling system are different – substantially, lower (180 °C) with auxiliary cooling compared to without cooling (330 °C) after 600 s of nitridation.
- OES Results (Fig. b):** shows three prominent peaks at 337, 316 and 358 nm corresponding to reactive N₂^{*}.
- Fig. c:** the peak intensity at 337 nm for p-Ni₃N is continuously enhanced with elongated time, however for cp-Ni₃N the peak intensity does not increase.
- Fig. d:** shows plasma parameters estimations for cp-Ni₃N using Langmuir probes. Plasma parameter (electron temperature and ion densities) which are significantly lower (more than half) than for p-Ni₃N.